



1 **Contributions of different sources to nitrous acid (HONO) at the SORPES**  
2 **station in eastern China: results from one-year continuous observation**

3  
4 Yuliang Liu<sup>1,2</sup>, Wei Nie<sup>1,2\*</sup>, Zheng Xu<sup>1,2</sup>, Tianyi Wang<sup>1,2</sup>, Ruoxian Wang<sup>1,2</sup>,  
5 Yuanyuan Li<sup>1,2</sup>, Lei Wang<sup>1,2</sup>, Xuguang Chi<sup>1,2</sup>, and Aijun Ding<sup>1,2</sup>

6  
7 <sup>1</sup>Joint International Research Laboratory of Atmospheric and Earth System Sciences, School  
8 of Atmospheric Sciences, Nanjing University, Nanjing, Jiangsu Province, China

9 <sup>2</sup>Collaborative Innovation Center of Climate Change, Jiangsu Province, China

10

11 **Abstract**

12

13 Nitrous acid (HONO), a reservoir of the hydroxyl radical (OH), has been  
14 long-standing recognized to be of significant importance to atmospheric chemistry,  
15 but its sources are still debate. In this study, we conducted continuous measurement of  
16 HONO from November 2017 to November 2018 at SORPES station in Nanjing of  
17 eastern China. The yearly average mixing ratio of observed HONO was  $0.69 \pm 0.58$   
18 ppb, showing a larger contribution to OH relative to ozone with a mean OH  
19 production rate of  $0.90 \pm 0.27$  ppb/h. To estimate the effect of combustion emissions  
20 of HONO, the emitted ratios of HONO and NO<sub>x</sub> were derived from 55 fresh plumes  
21 (NO/NO<sub>x</sub> > 0.85), with a mean value of 0.79%. The well-defined seasonal and diurnal  
22 patterns with clear wintertime and early morning concentration peaks of both HONO  
23 and NO<sub>x</sub> indicate that NO<sub>x</sub> is the critical precursor of HONO. During the nighttime,  
24 the chemistry of HONO was found to depend on RH, and heterogeneous reaction of  
25 NO<sub>2</sub> on aerosol surface was presumably responsible for HONO production. The  
26 average nighttime NO<sub>2</sub>-to-HONO conversion frequency ( $C_{\text{HONO}}$ ) was determined to  
27 be  $0.0055 \pm 0.0032$  h<sup>-1</sup> from 137 HONO formation cases. The missing source of  
28 HONO around noontime seemed to be photo-induced with an average  $P_{\text{unknown}}$  of  $1.13$   
29  $\pm 0.95$  ppb h<sup>-1</sup>, based on a semiquantitative HONO budget analysis. An  
30 over-determined system of equations was applied to obtain the monthly variations in  
31 nocturnal HONO sources. Except for burning-emitted HONO (approximately 23%  
32 of total measured HONO), the contribution of heterogeneous formation on ground  
33 surfaces was an approximately constant proportion of 36% throughout the year. The



34 soil emission revealed clear seasonal variation, and contributed up to 40% of observed  
35 HONO in July and August. A higher propensity for generating HONO on aerosol  
36 surface occurred in heavily polluted period (about 40% of HONO in January). Our  
37 results highlight ever-changing contributions of HONO sources, and encourage more  
38 long-term observations to evaluate the contribution from varied sources.

39

## 40 **1. Introduction**

41

42 Nitrous acid (HONO) is a vital constituent of nitrogen cycle in the atmosphere, first  
43 observed in the field by Perner and Platt (1979). The concentrations of HONO varied  
44 from dozens of ppt in remote regions (Villena et al., 2011b; Meusel et al., 2016) to  
45 several ppb in polluted urban regions (Yu et al., 2009; Tong et al., 2015). The  
46 photolysis of HONO (R1) has been long standing as a momentous source of the  
47 hydroxyl radical (OH) especially during the early morning when other OH sources are  
48 minor (Platt et al., 1980; Alicke, 2002, 2003). Even during the daytime, recent studies  
49 have recognized the photolysis of HONO as a potentially stronger contributor to  
50 daytime OH radical than that of O<sub>3</sub> (Kleffmann, 2005; Elshorbany et al., 2009; Li et al.,  
51 2018). Meanwhile, HONO has been found to affect adversely human health (Jarvis et  
52 al., 2005; Sleiman et al., 2010).

53

54 Although the significance of HONO has been given much weight, the sources of  
55 ambient HONO are complicated and have been debated for decades. HONO can be  
56 emitted from combustion, including vehicle exhaust, industrial exhaust and biomass  
57 burning (Table 1). Tunnel experiments with tests for different engine types have  
58 determined an emission ratio of HONO/NO<sub>x</sub> for traffic source, ranged in 0.3-0.8%  
59 (Kirchstetter et al., 1996; Kurtenbach et al., 2001). The release from soil nitrite  
60 through acidification reaction and partitioning is considered to be another primary  
61 source of atmospheric HONO (Su et al., 2011). Soil nitrite could come from  
62 biological nitrification and denitrification processes (Canfield et al., 2010; Oswald et  
63 al., 2013), or be enriched via reactive uptake of HONO from the atmosphere  
64 (VandenBoer et al., 2014a; VandenBoer et al., 2014b). In addition to direct emissions,



65 the vast majority of HONO is produced chemically. The recombination of NO and  
66 OH (R3) is the main homogeneous reaction for supplying HONO (Pagsberg et al.,  
67 1997;Atkinson, 2000), whose contribution may be significant under conditions of  
68 sufficient reactants during daytime. During the nighttime, with low OH concentrations,  
69 other larger sources, heterogeneous reactions of NO<sub>2</sub> on various surfaces, are required  
70 to explain elevated mixing levels of HONO. Laboratory studies indicate that NO<sub>2</sub> can  
71 be converted to HONO on humid surfaces (R4), being first order in NO<sub>2</sub> and  
72 depending on various parameters including the gas phase NO<sub>2</sub> concentration, the  
73 surface water content, and the surface area density (Kleffmann et al.,  
74 1998;Finlayson-Pitts et al., 2003). Besides, heterogeneous reduction of NO<sub>2</sub> with  
75 surface organics (R5) is proposed to be another effective pathway to generate HONO  
76 (Ammann et al., 1998;Ammann et al., 2005;Aubin and Abbatt, 2007), observed in  
77 freshly emitted plumes with high concentrations of NO<sub>x</sub> and BC (Xu et al., 2015).  
78 Notably this reaction rate is drastically reduced after the first few seconds due to  
79 consumption of the reactive surfaces (Kalberer et al., 1999;Kleffmann et al., 1999),  
80 but this reaction could be strongly enhanced by light on photo-activated surface  
81 (George et al., 2005;Stemmler et al., 2006;Stemmler et al., 2007). During the daytime,  
82 heterogeneous HONO formation from the photolysis of adsorbed nitric acid (HNO<sub>3</sub>)  
83 and particulate nitrate (NO<sub>3</sub><sup>-</sup>) at UV wavelengths has been found in experiments and  
84 observations (Zhou et al., 2003;Zhou et al., 2011;Ye et al., 2016;Ye et al., 2017).  
85 Heterogeneous processes are typically considered as the primary sources of HONO in  
86 many regions yet are the most poorly understood. For NO<sub>2</sub> conversion to HONO on  
87 surfaces (R4, R5), the uptake coefficients of NO<sub>2</sub> derived from different experiments  
88 vary from 10<sup>-9</sup> to 10<sup>-2</sup> (Ammann et al., 1998;Kirchner et al., 2000;Underwood et al.,  
89 2001;Aubin and Abbatt, 2007;Zhou et al., 2015). The key step to determine the  
90 uptake of NO<sub>2</sub> or the reaction rate is still ill-defined, and we are also not certain if and  
91 how the ambient natural surfaces can be reactivated by radiation. Furthermore, it has  
92 become a main concern to compare the contributions of ground and aerosol surfaces  
93 to HONO formation. It is so far, not well explained for the observed HONO,  
94 especially during daytime. Large unknown sources of HONO were identified by many



95 studies (Su et al., 2008b;Sörgel et al., 2011;Michoud et al., 2014;Lee et al., 2016).  
96  
97 Benefitting from more and more studies, particularly the observations under different  
98 environment (Lammel and Cape, 1996;Li et al., 2012), understanding of HONO  
99 chemistry in the atmosphere has been greatly improved during the last decade.  
100 However, most HONO observations were short-term campaigns with studies ranging  
101 from several weeks to several months. For example, Reisinger (2000) found a linear  
102 correlation between the HONO/NO<sub>2</sub> ratio and aerosol surface density in the polluted  
103 winter atmosphere, and Nie et al. (2015) showed the influence of biomass burning  
104 plumes on HONO chemistry, according to observed data during late April–June 2012,  
105 while Wong et al. (2011) believed that NO<sub>2</sub> to HONO conversion on the ground was  
106 the dominant source of HONO by analyzing vertical profiles from 15 August to 20  
107 September in 2006. Moreover, a theory that HONO from soil emission explained the  
108 strength and diurnal variations of the missing source has been presented by Su et al.  
109 (2011) based on data measured from 23 to 30 October 2004. In case the HONO  
110 sources possibly exhibit temporal variability, especially seasonal differences, it is  
111 challenging to draw a full picture on the basis of these short-term observations. More  
112 than a year of continuous observation is needed, yet rather limited.  
113  
114 The Yangtze River Delta (YRD) is one of the most developed regions in eastern  
115 China. Rapid urbanization and industrialization have induced severe air pollution over  
116 the last three decades, particularly high concentrations of reactive nitrogen (Richter et  
117 al., 2005;Rohde and Muller, 2015), including HONO (Wang et al., 2013;Nie et al.,  
118 2015). In this study, we conducted continuous HONO observations at the SORPES  
119 station (Station for Observation Regional Processes and the Earth System), located in  
120 the western part of the YRD, a place that can be influenced by air masses from  
121 different source regions of anthropogenic emissions, biomass burning, dust and  
122 biogenic emissions (Ding et al., 2013;Ding et al., 2016). Our observation was  
123 conducted continuously from November 2017 to November 2018 and showed  
124 well-defined diurnal patterns and obvious season variations of HONO concentrations



125 at relatively high levels. We discussed the potential mechanism of HONO production  
126 based upon semiquantitative analysis and correlation studies, and paying special  
127 attention to changes in major sources of HONO during different seasons.

128

## 129 **2. Methodology**

130

### 131 ***2.1. Study site and instrumentation***

132

133 Continuously observations was conducted at the SORPES station at the Xianlin  
134 Campus of Nanjing University (118°57'E, 32°07'N), located in the northeast suburb  
135 of Nanjing, China, from November 2017 to November 2018. The easterly prevailing  
136 wind and synoptic condition makes it a representative background site of Nanjing and  
137 a regional, downwind site of the city cluster in YRD region. Detailed descriptions for  
138 the station can be found in previous studies (Ding et al., 2013;Ding et al., 2016).

139

140 HONO was measured with a commercial long path absorption photometer instrument  
141 (QUMA, Model LOPAP-03). A brief description of this instrument is provided as  
142 follows. The ambient air was sampled in two similar temperature controlled stripping  
143 coils in series using a mixture reagent of 100 g sulfanilamide and 1 L HCl (37%  
144 volume fraction) in 9 L pure water. In the first stripping coil, almost all of the HONO  
145 and a fraction of interfering substances were absorbed into solution, and the  
146 remaining HONO and the most of the interfering species were absorbed in the second  
147 stripping coil. After adding a reagent of 1.6 g  
148 N-naphtylethylenediamine-dihydrochloride in 9 L pure water to both coils, colored azo  
149 dyewas formed in the solutions from 2 stripping coils, which were then separately  
150 detected via long path absorption in special Teflon tubing. The interference free  
151 HONO signal was the difference between the signals in the two channels. Further  
152 details can be found in (Heland et al., 2001;Kleffmann et al., 2006). To correct for the  
153 small drifts in instrument's baseline, compressed air was sampled every 12 h (flow  
154 rate: 1 L/min) to make zero measurement. A span check was made using 0.04 mg/m<sup>3</sup>  
155 nitrite (NO<sub>2</sub><sup>-</sup>) solution each weeks with a flow rate of 0.28 ml/min. The time



156 resolution, detection limit, accuracy of the measurement was 10 min, 5 pptv, and 10%,  
157 respectively.

158

159 The NO and NO<sub>2</sub> levels were measured using a chemiluminescence instrument (TEI,  
160 model 42i) coupled with a highly selective photolytic converter (Droplet  
161 Measurement Technologies, model BLC), and the analyzer had a detection limit of 50  
162 pptv for an integration time of 5 min, with precision of 4% and an uncertainty of 10%  
163 (Xu et al., 2013). O<sub>3</sub> and CO were measured continuously using Thermo-Fisher  
164 Scientific TEI 49i and TEI 48i. The fine particle mass concentration (PM<sub>2.5</sub>) was  
165 continuously measured with a combined technique of light scattering photometry and  
166 beta radiation attenuation (Thermo Scientific SHARP Monitor Model 5030). Water  
167 soluble aerosol ions (NO<sub>3</sub><sup>-</sup>, SO<sub>4</sub><sup>2-</sup>, NH<sub>4</sub><sup>+</sup> etc.) and ammonia (NH<sub>3</sub>) were measured by a  
168 Monitor for Aerosols and Gases in ambient Air (designed and manufactured by  
169 Applikon Analytical B.V., the Netherlands) with a PM<sub>2.5</sub> cyclone inlet, in a time  
170 resolution of 1 hr. The size distribution of submicron particles (6-820 nm) is measured  
171 with a DMPS (differential mobility particle sizer) constructed at the University of  
172 Helsinki in Finland. Meteorological measurements including relative humidity (RH),  
173 wind speed, wind direction, and air temperature were recorded by Automatic Weather  
174 Station (CAMPEEL co., AG1000). UVB total radiation was measured by UVB  
175 radiometer (UVS-B-T UV Radiometer, KIPP & ZONEN).

176

## 177 **2.2. TUV model and OH estimate**

178

179 The Tropospheric Ultraviolet and Visible (TUV) Radiation Model ([http://www.acd.  
180 ucar.edu/TUV](http://www.acd.ucar.edu/TUV)) was adopted to compute the photolysis frequencies, which is  
181 most probably accurate in clean and cloudless days. The pivotal parameters of this  
182 model were inputted as follows: the ozone density was measured by Total Ozone  
183 Mapping Spectrometer (<http://toms.gsfc.nasa.gov/teacher/ozoneoverhead.html>); the  
184 typical single scattering albedo (SSA) and Ångström exponent (Alpha) were 0.93  
185 and 1.04 (Shen et al., 2018); the mean value of optical depth (AOD) at 550 nm was  
186 0.640, derived following an empirical relationship with PM<sub>2.5</sub> in Nanjing (Shao et



187 al., 2017). To reduce the error of model, we used observed UVB to correct simulated  
188 results ( $J_{\text{mod}}$ ) by Eq. (1). The daytime OH concentration was calculated by applying  
189 the linear fitting formula (Eq. 2) that obtained from correlations of measured OH  
190 concentrations with simultaneously observed  $J(\text{O}^1\text{D})$ , suggested by Rohrer and  
191 Berresheim (2006). The calculated OH concentrations around noon were in the range  
192 of  $0.15\text{--}1.17 \times 10^7 \text{ cm}^{-3}$ , comparable to observations in Chinese urban atmospheres (Lu  
193 et al., 2012; Lu et al., 2013).

194

$$195 \quad J = \frac{\text{UVB}_{\text{obs}}}{\text{UVB}_{\text{mod}}} J_{\text{mod}} \quad (1)$$

$$196 \quad [\text{OH}] = a \times (J(\text{O}^1\text{D}) / 10^{-5} \text{ s}^{-1})^b + c \quad (2)$$

( $a = 2.4 \times 10^6 \text{ cm}^{-3}$ ,  $b = 1$ ,  $c = 0.13 \times 10^6 \text{ cm}^{-3}$ )

197

### 198 **3. Results**

199

#### 200 **3.1. Observation overview**

201

202 We carried out continuous measurements for HONO at SORPES station in the  
203 northeast suburb of Nanjing from November 2017 to November 2018 with a mean  
204 measured ambient HONO mixing level of  $0.69 \pm 0.58$  ppb, within the range of those  
205 in or in the vicinity of mega cities (Table 2). Fig. 1 shows the seasonal pattern of  
206 HONO and related parameters. The highest concentration of HONO was found in  
207 winter ( $1.04 \pm 0.75$  ppb), followed by spring ( $0.68 \pm 0.48$  ppb), autumn ( $0.66 \pm 0.53$   
208 ppb) and summer ( $0.45 \pm 0.37$  ppb). Such seasonal variations in Nanjing are aligned  
209 with that in Beijing (Hendrick et al., 2014), and are somewhat similar to those in Jinan  
210 (Li et al., 2018), where the highest levels occurred in winter and the lowest levels  
211 occurred in autumn, but these variations are different from those in Hongkong (Xu et  
212 al., 2015) where the highest and lowest values of HONO appeared in autumn and  
213 spring, respectively. The important point is that the seasonality of HONO coincides  
214 with that of  $\text{NO}_x$  (or  $\text{NO}_2$ ), which is believed to be the main precursor of HONO, in  
215 current studies.

216



217 The HONO to  $\text{NO}_x$  ratio or the HONO to  $\text{NO}_2$  ratio has been used extensively in  
218 previous research to characterize the HONO levels and to indicate the extent of  
219 heterogeneous conversion of  $\text{NO}_2$  to HONO, since it is less influenced by convection  
220 or transport processes than the individual concentration (Lammel and Cape,  
221 1996;Stutz et al., 2002). When a large proportion of HONO comes from direct  
222 emissions, the value of HONO/ $\text{NO}_2$  usually becomes larger, falsely implying the  
223 strong formation of HONO from  $\text{NO}_2$ , however, the freshly emitted air masses  
224 generally have the lowest HONO/ $\text{NO}_x$  ratio, meaning that HONO/ $\text{NO}_x$  behaves better  
225 than HONO/ $\text{NO}_2$  in a way. As shown in Fig. 1(b), the low value of HONO/ $\text{NO}_x$  in  
226 winter is attributed to heavy emissions because we see high mixing ratios of NO  
227 during this cold season (Fig. 1c), the reasons for two peaks of HONO/ $\text{NO}_x$  in spring  
228 and summer will be discussed in sections 3.3, 3.4 and 4.

229

230 All daily changes of HONO concentration in different seasons closely resemble a  
231 cycle in which HONO peaks in the early morning, and then decreases to the minimum  
232 at dusk, following the diurnal trend of  $\text{NO}_x$  (Fig. 2). The daily variations of HONO in  
233 Nanjing are like those seen in other urban areas (Villena et al., 2011a;Wang et al.,  
234 2013;Michoud et al., 2014;Lee et al., 2016), but differ from observations on the  
235 roadside (Rappenglück et al., 2013;Xu et al., 2015). At night, the mixing ratio of  
236 HONO increases rapidly in the first few hours and then stabilizes (in spring and  
237 summer) or gradually climbs to its peak in the morning rush hour (in winter and  
238 autumn). The accumulation during nighttime hours suggests a significant production  
239 of HONO exceeding the dry deposition of HONO. As the sun rises, the HONO sink  
240 will be strengthened by photolysis and the vertical mixing of HONO. It's clear that the  
241 peak times varying seasonally result from different sunrise times. During the daytime,  
242 the rate of HONO abatement is rapid before noon and then becomes progressively  
243 until HONO concentration falling to the minimum. Given that the photolytic lifetime  
244 of HONO is about 10-20 min in the midday (Stutz et al., 2000), the considerable  
245 HONO concentration during daytime indicates the existence of large sources of  
246 HONO production.



247

248 From the daily variations of the HONO to NO<sub>x</sub> ratio, we can further understand the  
249 behavior of HONO in the atmosphere. HONO/NO<sub>x</sub> is regularly enhanced quickly  
250 before midnight then reaches a maximum during the latter half of the night.  
251 According to Stutz et al. (2002), the highest HONO/NO<sub>x</sub> (or HONO/NO<sub>2</sub>) is defined  
252 by the balance between production and loss of HONO at each night, the conditions  
253 affecting the maximum ratio at nighttime will be discussed in section 3.3. What's  
254 interesting here is the peak of the HONO/NO<sub>x</sub> ratio in the midday sun in spring,  
255 summer and autumn, and even in winter, the ratio doesn't decline but remains  
256 stationary before and at noon. If the HONO sources during daytime are consistent  
257 with those at night, the minimum HONO/NO<sub>x</sub> ratios should occur at noon due to the  
258 intense photochemical loss of HONO. Therefore, there must be additional sources of  
259 HONO during daytime. The increase of HONO/NO<sub>x</sub> with solar radiation (e.g., UVB)  
260 is found in both diurnal and seasonal variations, indicating that these daytime sources  
261 have a relationship with the intensity of solar radiation. We will further discuss the  
262 potential daytime sources of HONO in section 3.4.

263

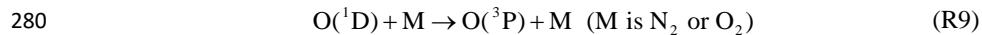
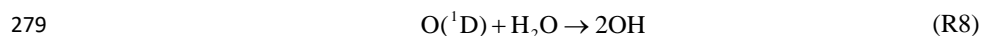
264 The elevated mixing ratio of HONO presents an efficient reservoir of OH radicals  
265 during daytime in Nanjing. We calculate the net OH production rate from HONO  
266  $P_{OH}(\text{HONO})$  using Eq. (3) (Li et al., 2018). For comparison, the OH production rate  
267 from ozone photolysis,  $P_{OH}(\text{O}_3)$ , is also derived from Eq. (4). Based on Alicke et al.  
268 (2002) and Alicke (2003), only part of the O(<sup>1</sup>D) atoms, formed by the photolysis of  
269 O<sub>3</sub> at wavelengths below 320 nm (R7), can produce OH radicals by reacting with  
270 water (R8) in the atmosphere, so we use the absolute water concentration, which can  
271 be derived from relative humidity and temperature, to calculate the branching ratio of  
272 O(<sup>1</sup>D) ( $\Phi_{OH}$ ) between R8 and R9. The reaction rate of O(<sup>1</sup>D) with O<sub>2</sub> is  $4.0 \times 10^{-11} \text{ cm}^3$   
273  $\text{molecules}^{-1} \text{ s}^{-1}$  and the reaction rate of O(<sup>1</sup>D) with N<sub>2</sub> is  $3.1 \times 10^{-11} \text{ cm}^3 \text{ molecules}^{-1}$   
274  $\text{s}^{-1}$  (Seinfeld and Pandis, 2016).

275



$$\begin{aligned}
 P_{\text{OH}}(\text{HONO}) &= J(\text{HONO})[\text{HONO}] - k_{\text{NO}+\text{OH}}[\text{NO}][\text{OH}] \\
 &\quad - k_{\text{HONO}+\text{OH}}[\text{HONO}][\text{OH}]
 \end{aligned}
 \tag{3}$$

$$\begin{aligned}
 P_{\text{OH}}(\text{O}_3) &= 2J(\text{O}^1\text{D})[\text{O}_3]\phi_{\text{OH}} \\
 \phi_{\text{OH}} &= k_8[\text{H}_2\text{O}] / (k_8[\text{H}_2\text{O}] + k_9[\text{M}])
 \end{aligned}
 \tag{4}$$



281

282 Fig. 3 shows that the diurnal peak of OH production rate from HONO is usually found  
 283 in the late morning, caused by the combined effects of HONO concentration and its  
 284 photolysis frequency,  $J_{\text{HONO}}$ , and the seasonal peak of  $P_{\text{OH}}(\text{HONO})$  occurs in spring  
 285 for the same reason.  $P_{\text{OH}}(\text{O}_3)$ , coinciding with the trend of  $J(\text{O}^1\text{D})$ , is highest around  
 286 noon and in summer at daily and seasonal time scale respectively. Significantly, the  
 287 photolysis of HONO produced more OH than that of ozone throughout the daytime in  
 288 winter, spring and autumn. In summer, the contribution of HONO to OH is greater in  
 289 the early morning, and, although the photolysis of ozone contributes more OH at noon,  
 290 the role of HONO is considerable. Overall, the average  $P_{\text{OH}}(\text{HONO})$  during  
 291 8:00-16:00 LT is  $0.90 \pm 0.27$  ppb/h, more than twice the value of  $P_{\text{OH}}(\text{O}_3)$ , the mean  
 292 value of which is  $0.41 \pm 0.25$  ppb/h. The impressive role of HONO in the atmospheric  
 293 oxidizing capacity should benefit photochemical ozone production (Ding et al.,  
 294 2013; Xu et al., 2017; Xu et al., 2018), new particle formation (Qi et al., 2015) and  
 295 secondary aerosol formation (Xie et al., 2015; Sun et al., 2018) in Nanjing, the western  
 296 YRD region.

297

### 298 **3.2. Direct emissions of HONO from Combustion**

299

300 As mentioned above and shown in Fig. 4(a), the similar patterns of HONO and  $\text{NO}_x$ ,  
 301 particularly sharply increasing together in the fresh plumes, in which the  $\text{NO}/\text{NO}_x$   
 302 ratios are usually very high, indicate the presence of direct combustion emission of  
 303 HONO, which need to be deducted when analyzing the secondary formation of



304 HONO. The SORPES station are influenced by air masses from both industries and  
305 vehicles (Ding et al., 2016), the traffic emission factor investigated in other  
306 experiments cannot be used straightly; thus, we derive the emitted HONO/NO<sub>x</sub> ratio  
307 according the method of Xu et al. (2015), and the following five criteria are adopted  
308 to choose fresh plumes : (a) NO<sub>x</sub>>40ppbv; (b)  $\Delta\text{NO}/\Delta\text{NO}_x>0.85$ ; (c) good  
309 correlation between HONO and NO<sub>x</sub> ( $r>0.9$ ); (d) short duration of plumes ( $\leq 2$  h);  
310 and (e) UVB $\leq 0.01$  W/m<sup>2</sup>. Then, the slopes of HONO to NO<sub>x</sub> in selected plumes  
311 were considered as the emission ratios in our study.

312

313 Within the one-year dataset, we selected 55 freshly emitted plumes satisfying the  
314 criteria above (Table 3), of which 20 air masses were found in the morning and  
315 evening rush hours; the derived  $\Delta\text{HONO}/\Delta\text{NO}_x$  ratios vary from 0.26% to 1.91%  
316 with a mean value of  $0.79\% \pm 0.36\%$ . Many factors, such as the amount of excess  
317 oxygen; the types of fuel used (gasoline, diesel, coal); if engines are catalyst-equipped,  
318 and if engines are well-maintained, could result in variances in these ratios.  
319 Additionally, the rapid heterogeneous reduction of NO<sub>2</sub> on synchronously emitted BC  
320 can also raise the value of  $\Delta\text{HONO}/\Delta\text{NO}_x$  (Xu et al., 2015). For our study,  
321 an average emission factor of 0.79% is deployed to evaluate the emission contribution  
322 of HONO (Eq. 5), which is abbreviated as HONO<sub>emis</sub>.

323

$$324 \quad \text{HONO}_{\text{emis}} = \text{NO}_x \times 0.0079 \quad (5)$$

$$325 \quad \text{HONO}_{\text{corr}} = \text{HONO} - \text{HONO}_{\text{emis}} \quad (6)$$

326

327 Combustion emissions contribute an average of 23% of total measured HONO  
328 concentrations at night (Fig. 4b), with a maximum HONO<sub>emis</sub>/HONO value of 32% in  
329 winter and a minimum HONO<sub>emis</sub>/HONO value of 18% in summer. We then get the  
330 corrected observed HONO (HONO<sub>corr</sub>) by Eq. (6) for further analysis. The slope of  
331 the fitted line for HONO and NO<sub>x</sub> is 1.62%, higher than emission ratio 0.79% (Fig.  
332 4a), and almost 80% of HONO is from HONO<sub>corr</sub> that is not affected by emissions  
333 (Fig. 4b). These imply significant secondary formation of HONO in the atmosphere.



334

335 **3.3. Heterogeneous conversion of NO<sub>2</sub> to HONO during nighttime**

336

337 **3.3.1. The NO<sub>2</sub>-to-HONO conversion rate (C<sub>HONO</sub>)**

338

339 In addition to emissions, heterogeneous reaction of NO<sub>2</sub> on surfaces (R4, R5) is  
340 believed to be the major formation pathway of nocturnal HONO. Thus, the  
341 NO<sub>2</sub>-to-HONO conversion frequency is calculated from Eq. (5) (Alicke et al.,  
342 2002; Alicke, 2003; Wentzell et al., 2010), where NO<sub>2</sub> is adopted to scale HONO to  
343 reduce the dilution influence according to Su et al. (2008a). Similar to HONO/NO<sub>x</sub>  
344 (Fig. 2), the nighttime HONO<sub>corr</sub>/NO<sub>2</sub> ratio rises from the lowest value and then  
345 reaches a quasi-stable state, meaning that C<sub>HONO</sub> can actually be used to assess how  
346 quickly HONO<sub>corr</sub>/NO<sub>2</sub> increases to its equilibrium.

347

$$348 \quad C_{\text{HONO}} = \frac{\frac{[\text{HONO}_{\text{corr}}]_{(t_2)} - [\text{HONO}_{\text{corr}}]_{(t_1)}}{[\text{NO}_2]_{(t_2)}}}{t_2 - t_1} \quad (7)$$

349

350 Following the method of Xu et al. (2015) and Li et al. (2018), 137 cases in which  
351 HONO<sub>corr</sub>/NO<sub>2</sub> increased almost linearly from 18:00 to 24:00 each night are selected,  
352 and the slope fitted by the least linear regression for HONO<sub>corr</sub>/NO<sub>2</sub> against time is  
353 just the conversion frequency of NO<sub>2</sub> to HONO. The derived C<sub>HONO</sub> vary from 0.0043  
354 ± 0.0017 h<sup>-1</sup> in winter to 0.0066 ± 0.0040 h<sup>-1</sup> in summer, with an average value of  
355 0.0055 ± 0.0032 h<sup>-1</sup>, which is in the range (0.044-0.014 h<sup>-1</sup>) shown by other studies in  
356 urban and suburban sites (Fig. 5). Noting that C<sub>HONO</sub> assumes the increase of  
357 HONO<sub>corr</sub>/NO<sub>2</sub> is caused by the conversion of NO<sub>2</sub>, excluding other possible sources  
358 of HONO (e.g. soil nitrite); and the computed C<sub>HONO</sub> is the net NO<sub>2</sub>-to-HONO  
359 conversion rate since the measured HONO<sub>corr</sub> has already taken in to account the sinks  
360 of HONO (mainly deposition). Considering the uncertainties of C<sub>HONO</sub>, utilizing  
361 C<sub>HONO</sub> directly to analyze the mechanism of HONO formation may not be appropriate,  
362 but it could be attemptable to facilitate the parameterizations for HONO production in  
363 air quality models by C<sub>HONO</sub>.



364

365 **3.3.2. RH dependence of HONO chemistry**

366

367 It appears that NO<sub>2</sub> hydrolysis on humid surfaces (R4), having a first order  
368 dependence on NO<sub>2</sub> (Jenkin et al., 1988; Ackermann, 2000; Finlayson-Pitts et al.,  
369 2003), is influenced by the surface absorbed water rather than by atmospheric water  
370 vapor (Kleffmann et al., 1998; Finlayson-Pitts et al., 2003), although the exact  
371 mechanisms are still unknown. In the studies of Stutz et al. (2002) and Stutz et al.  
372 (2004), the pseudo steady state of HONO/NO<sub>2</sub>, where this ratio is at a maximum, is  
373 presumed to be a balance between the production of HONO from NO<sub>2</sub> and the loss of  
374 HONO on surfaces, and the highest HONO/NO<sub>2</sub> is determined by the ratio of the  
375 reactive uptake coefficients for each process. Scatter plot of HONO<sub>corr</sub>/NO<sub>2</sub> against  
376 relative humidity in our study are illustrated in Fig. 5; to eliminate the influence of  
377 other factors as far as possible, the average of the 6 highest HONO<sub>corr</sub>/NO<sub>2</sub> values in  
378 each 5% RH interval is calculated, according to Stutz et al. (2004).

379

380 The phenomenon that HONO<sub>corr</sub>/NO<sub>2</sub> first increases and then decreases with an  
381 increasing RH in Fig. 5(a) was also observed by other studies (Hao et al., 2006; Yu et  
382 al., 2009; Li et al., 2012; Wang et al., 2013). In addition, the trend that HONO<sub>corr</sub>/NO<sub>2</sub>  
383 increases roughly with RH except when RH values are greater than 95%, as shown in  
384 Fig. 5(b), is also found in Stutz et al. (2004) and Qin et al. (2009). The dependencies  
385 of HONO<sub>corr</sub>/NO<sub>2</sub> on RH and the possible reasons or mechanisms are discussed as  
386 follows. Even at the lowest measured RH of 18%, the absolute moisture content in the  
387 atmosphere is still greater than 10<sup>3</sup> ppm in our study, but the HONO<sub>corr</sub>/NO<sub>2</sub> ratio is  
388 quite small and remains unchanged when RH is below 45%, indicating that the NO<sub>2</sub>  
389 to HONO conversion efficiency should be determined by water covering the surfaces,  
390 and HONO is seemingly produced on "dry" surfaces where the amount of  
391 chemisorbed water becomes approximately independent on the water vapor levels  
392 in dry conditions, according to Lammel (1999).

393

394 It has been reported that surface absorbed water depends on RH values, and the



395 dependences vary for different material surfaces of the ground, but generally follow  
396 the shape of a BET isotherm (Lammel, 1999;Saliba et al., 2001;Sumner et al., 2004).  
397 The number of mono-layers of water increases slowly from zero to 2-4, accompanied  
398 by RH from 0 to a turning point, and the water coverage grows dramatically (up to  
399 10-100 mono-layers) once RH exceeds the turning point (Finlayson-Pitts et al., 2003).  
400 Fig. 5(a) shows the case where the surface for NO<sub>2</sub> converting to HONO is dominated  
401 by the ground, the HONO<sub>corr</sub>/NO<sub>2</sub> increases along with RH when RH is less than 75%,  
402 which can be explained by the reaction of NO<sub>2</sub> to generate HONO on wet surfaces.  
403 However, a negative correlation between HONO<sub>corr</sub>/NO<sub>2</sub> and RH is found when RH is  
404 over 75%, presumably because the rapidly growing aqueous layers of the ground  
405 surface lead to efficient uptake of HONO and make the surface less accessible or less  
406 reactive for NO<sub>2</sub>. Hence, the RH turning point for absorbed water on ground surfaces  
407 is perhaps around 75% for our observation, within the range of results from  
408 experiments on various surfaces (70-80% RH) (Lammel, 1999;Saliba et al.,  
409 2001;Sumner et al., 2004). Once RH exceeds 95%, the reaction surface is classified as  
410 an “aqueous” surface in Lammel (1999), asymptotically approaching the state of  
411 water droplet. Under these circumstances, the efficiency of NO<sub>2</sub> forming HONO will  
412 be reduced since the conversion has changed from a "heterogeneous reaction" to a  
413 "liquid reaction" (Lee and Schwartz, 1981;Cheung et al., 2000;Kleffmann et al.,  
414 1998;Finlayson-Pitts and Pitts Jr, 1999), and the aqueous surface is found to be an  
415 impactful sink of HONO in experimental work (Park and Lee, 1988;Becker et al.,  
416 1996;Hirokawa et al., 2008) and in field observations(Acker et al., 2005;He et al.,  
417 2006;Zhou et al., 2007). For the reasons mentioned above, we can see a dramatic  
418 decline of HONO<sub>corr</sub>/NO<sub>2</sub> in Fig. 5(a) and Fig. 5(b) when RH approaches 100%.  
419  
420 Especially deserving of mention, the constant HONO<sub>corr</sub>/NO<sub>2</sub> value with RH ranging  
421 from 75% to 95% under the condition of high PM<sub>2.5</sub> mass loading (Fig. 5(b)) ,  
422 compared to the downward trend of HONO<sub>corr</sub>/NO<sub>2</sub> within the same humidity range in  
423 low PM<sub>2.5</sub> mass concentration (Fig. 5(a)), implies a contribution of aerosol surfaces to  
424 the NO<sub>2</sub>-HONO conversion. Since both HONO<sub>corr</sub>/NO<sub>2</sub> in Fig. 5(a) and Fig. 5(b) are



425 affected by the ground surfaces, we can use the difference of  $\text{HONO}_{\text{corr}}/\text{NO}_2$  between  
426 Fig. 5(a) and Fig. 5(b) to represent the influence of aerosol. As the area of shadow  
427 shown in Fig. 5(b), the aerosol-affected  $\text{HONO}_{\text{corr}}/\text{NO}_2$  is positively related to RH  
428 positively before RH reaches 95%, which is consistent with the results from  
429 laboratory studies that the uptake coefficient of  $\text{NO}_2$  to HONO ( $\gamma_{\text{NO}_2 \rightarrow \text{HONO}}$ ) increases  
430 with RH (Kleffmann et al., 1999; Liu et al., 2015). We will discuss the effect of  
431 aerosol on HONO production in the next part.

432

### 433 ***3.3.3. Impact of aerosols on HONO formation***

434

435 To further understand the heterogeneous formation of HONO on aerosol, we provide  
436 a correlation analysis of the related  $\text{HONO}_{\text{corr}}$  parameters ( $\text{HONO}_{\text{corr}}$  and  
437  $\text{HONO}_{\text{corr}}/\text{NO}_2$ ) with  $\text{PM}_{2.5}$  when  $\text{HONO}_{\text{corr}}/\text{NO}_2$  reaches the pseudo steady state each  
438 night (3:00-6:00 LT). The convergence or diffusion processes of gases and particles  
439 caused by the decrease or increase of the boundary layer height can also lead to a  
440 consistent trend of  $\text{HONO}_{\text{corr}}$  and  $\text{PM}_{2.5}$  (Fig. 6a), while the ratio of HONO and  $\text{NO}_2$   
441 can not only remove this physical effect to a certain extent but also represent the  
442 conversion degree of  $\text{NO}_2$  to HONO, so a moderate positive correlation between  
443  $\text{HONO}_{\text{corr}}/\text{NO}_2$  and  $\text{PM}_{2.5}$  ( $r=0.35$ ,  $p=0.01$ ) throughout the observation period could  
444 be more convincing (Fig. 6b). As shown by larger triangles with gray borders in Fig.  
445 6(b),  $\text{HONO}_{\text{corr}}/\text{NO}_2$  is better correlated with  $\text{PM}_{2.5}$  in the months during which the  
446 mass concentrations of  $\text{PM}_{2.5}$  are higher during this 1-year measurement, generally  
447 occurring from November to May (Fig. 1d). This finding can be explained with a law  
448 that greater contributions of  $\text{NO}_2$  heterogeneously reacting on aerosol to generate  
449 HONO lead to better correlations between  $\text{HONO}_{\text{corr}}/\text{NO}_2$  and  $\text{PM}_{2.5}$ . Interestingly,  
450 this relationship can also be divided approximately into two groups by  $\text{NH}_3/\text{CO}$ ; the  
451 correlation is good when the value of  $\text{NH}_3/\text{CO}$  is lower than 2%, but when  $\text{NH}_3/\text{CO}$  is  
452 higher than 2%, a poor correlation is found. We will discuss this phenomenon further  
453 in section 4. The evidence of HONO formation on aerosol were also found in other  
454 observations (Reisinger, 2000; Wang, 2003; Li et al., 2012; Nie et al., 2015; Hou et al.,  
455 2016; Cui et al., 2018).



456

457 As is known, producing HONO is not the dominant sink of NO<sub>2</sub> at night, but it seems  
458 that more NO<sub>2</sub> can be converted to HONO under conditions of heavy pollution (Fig.  
459 7b). We discuss whether heterogeneous reactions of NO<sub>2</sub> on aerosols are able to  
460 provide comparable HONO with our measurement by Eq. (8), where we only consider  
461 HONO formation on particle surfaces and assume that HONO principally settles on  
462 the ground surface, neglecting HONO loss on aerosol.  $c_{\text{NO}_2}$  is the mean molecular  
463 velocity of NO<sub>2</sub> (370 ms<sup>-1</sup>);  $[\frac{S}{V}]_{\text{aer}}$  is the surface area to volume ratio (m<sup>-1</sup>) of aerosol;  
464  $v_{\text{HONO}}$  is the deposition velocity of HONO, which is considered to be close to the  
465 deposition velocity of NO<sub>2</sub> at night (Stutz et al., 2002; Su et al., 2008a); and a  
466 approximate value of 0.1 cms<sup>-1</sup> is used based on the measurements from Coe and  
467 Gallagher (1992) and Stutz et al. (2002); H is the boundary layer mixing depth, and a  
468 value of 100 m is assumed for nighttime (Su et al., 2008a).

469

$$470 \quad C_{\text{HONO}} = \frac{1}{4} \gamma_{\text{NO}_2 \rightarrow \text{HONO}} c_{\text{NO}_2} \left[ \frac{S}{V} \right]_{\text{aer}} - \frac{v_{\text{HONO}}}{H} \frac{[\text{HONO}]}{[\text{NO}_2]} \quad (8)$$

471

472 Considering at nighttime period with severe haze, the aerosol surface density  
473 calculated from the particle number size distributions between 6 nm and 800 nm is  
474 about  $1.2 \times 10^{-3} \text{ m}^{-1}$ , matched by 200  $\mu\text{g}/\text{m}^3$  of PM<sub>2.5</sub> from our observations, and the  
475 averaged mixing ratios of HONO and NO<sub>2</sub> are 1.15 ppb and 28.4 ppb, respectively, at  
476 night in winter (Table 2). For 30% of the measured mean winter  $C_{\text{HONO}}$  (0.0013 h<sup>-1</sup>),  
477 the uptake coefficient of NO<sub>2</sub>-to-HONO ( $\gamma_{\text{NO}_2 \rightarrow \text{HONO}}$ ) is  $6.9 \times 10^{-6}$ , derived from Eq. (8),  
478 and for all of the measured mean winter  $C_{\text{HONO}}$  (0.0043 h<sup>-1</sup>) value, the  $\gamma_{\text{NO}_2 \rightarrow \text{HONO}}$  is 1.44  
479  $\times 10^{-5}$ , fitting the results from many laboratory studies which demonstrate that the  
480 uptake coefficients of NO<sub>2</sub> ( $\gamma_{\text{NO}_2}$ ) on multiple aerosol surfaces or wet surfaces are  
481 mainly distributed around  $10^{-5}$  with the HONO yield varying from 0.1 to 0.9 (Grassian,  
482 2002; Aubin and Abbatt, 2007; Khalizov et al., 2010; Han et al., 2017). It is necessary



483 to elaborate that: (1) the ambient particles were dried with silica gel before measuring  
484 their number size distributions, and the mass concentrations of PM<sub>2.5</sub> were also  
485 measured under a system where the temperature was maintained at 30 °C; (2) the  
486 aerosol surface was calculated using an assumption that all particles are spherically  
487 shaped, but the particles could in fact have irregular bodies and porous structure; (3)  
488 the particle size of both PM<sub>2.5</sub> and derived  $[\frac{S}{V}]_{\text{aer}}$  is just a part of the total suspended  
489 particulate matter. As described, the aerosol loading in the atmosphere is actually  
490 underestimated in our study, thus the  $\gamma_{\text{NO}_2 \rightarrow \text{HONO}}$  we derived could be the upper limit of  
491 the uptake coefficient for NO<sub>2</sub> conversion to HONO on aerosol. In addition to  
492 particles surfaces, other aerosol parameters such as surface water content, chemical  
493 composition, pH value, and phase state of surfaces may also influence the  
494 heterogeneous formation of HONO.

495

#### 496 **3.4. Missing daytime HONO source**

497

498 After discussing the nocturnal formation mechanism of HONO, we now focus on  
499 the chemistry of daytime HONO whose lifetime is only 10-20 min but whose  
500 concentrations are still about 0.25-0.6 ppb at noon (Fig. 2). We are not certain if the  
501 observed HONO can be provided by known mechanisms (gas phase reaction (R4) and  
502 emissions) to date, so a budget equation of daytime HONO (Eq. 9) is utilized to  
503 analyze its source and sinks (Su et al., 2008b; Sörgel et al., 2011). Here, dHONO/dt is  
504 the change rate of the observed HONO. The sources rates of HONO contain the  
505 homogeneous formation rate (P<sub>NO+OH</sub>, R4); the combustion emission rate (P<sub>emis</sub>); and  
506 the unknown HONO daytime source (P<sub>unknown</sub>). The sink rates of HONO consist of the  
507 photolysis rate (L<sub>phot</sub>, R1); the reaction rate of HONO with OH (L<sub>HONO+OH</sub>, R2); and  
508 the dry deposition rate (L<sub>dep</sub>). T<sub>v</sub> and T<sub>h</sub> represent the vertical (T<sub>v</sub>) and horizontal (T<sub>h</sub>)  
509 transport processes of HONO, which are thought to be negligible for intense radiation  
510 and relatively homogeneous atmospheres with generally calm winds (Dillon, 2002; Su  
511 et al., 2008b; Sörgel et al., 2011).

512



$$513 \quad \frac{d\text{HONO}}{dt} = (P_{\text{NO+OH}} + P_{\text{emis}} + P_{\text{unknown}}) - (L_{\text{phot}} + L_{\text{HONO+OH}} + L_{\text{dep}}) + T_v + T_h \quad (9)$$

514

515 Therefore, the undiscovered daytime source of HONO ( $P_{\text{unknown}}$ ) can be derived by Eq.  
 516 (10), which is a deformation of Eq. (9) without minor terms ( $T_v$  and  $T_h$ ) and where  
 517  $d\text{HONO}/dt$  is substituted by  $\Delta\text{HONO}/\Delta t$  that is counted as difference between  
 518 observed HONO at two time points. The reaction rate constants of reaction 2  
 519 ( $k_{\text{HONO+OH}}$ ) and reaction 4 ( $k_{\text{NO+OH}}$ ) are  $6.0 \times 10^{-12} \text{ cm}^3 \text{ molecules}^{-1} \text{ s}^{-1}$  and  $9.8 \times 10^{-12}$   
 520  $\text{ cm}^3 \text{ molecules}^{-1} \text{ s}^{-1}$ , respectively (Atkinson et al., 2004). The emission ratio of  
 521 HONO and  $\text{NO}_x$  ( $\text{HONO}/\text{NO}_x = 0.79\%$ ) obtained in section 3.2, is used to estimate  
 522  $P_{\text{emis}}$ . For  $L_{\text{dep}}$ , the dry deposition velocity of diurnal HONO ( $v_{\text{HONO}}$ ) is measured as 2  
 523  $\text{ cm s}^{-1}$  in the work of Harrison et al. (1996), and a practical mixing height of 200 m is  
 524 adopted, considering that most of the HONO cannot rise above this altitude due to  
 525 rapid photolysis (Alicke et al., 2002).

526

$$527 \quad P_{\text{unknown}} = J(\text{HONO})[\text{HONO}] + k_{\text{HONO+OH}}[\text{HONO}][\text{OH}] + \frac{v_{\text{HONO}}}{H}[\text{HONO}]$$

$$+ \frac{\Delta\text{HONO}}{\Delta t} - k_{\text{NO+OH}}[\text{NO}][\text{OH}] - \frac{0.79\% \times \Delta\text{NO}_x}{\Delta t} \quad (10)$$

528

529 Fig. 8 shows the average daytime HONO budget from 8:00 LT to 16:00 LT during  
 530 different seasons. The major loss route of HONO is photodecomposition ( $L_{\text{phot}}$ ) with  
 531 an average value of 1.32 ppb/h at noontime (10:00-14:00 LT) during this observation  
 532 period, next to dry deposition ( $L_{\text{dep}}$ ) whose mean value at the same time is 0.17 ppb/h,  
 533 and by  $L_{\text{HONO+OH}}$  which is less than 3% of that of  $L_{\text{phot}}$ . For the sources of HONO  
 534 around noon, the average homogeneous reaction rate between NO and OH ( $P_{\text{NO+OH}}$ ) is  
 535 0.32 ppb/h and  $P_{\text{emis}}$  just gives a tiny part of HONO at a rate of 0.02 ppb/h, meaning  
 536 that most HONO comes from an unknown source whose average rate ( $P_{\text{unknown}}$ ) is  
 537 1.13 ppb/h, contributing 76% of the production of HONO. Comparing summer data,  
 538 the mean unknown daytime source strength of HONO in Nanjing is almost at the  
 539 upper-middle level of those reported in the existing literature: 0.22 ppb/h at a rural  
 540 site of New York state, USA (Zhou et al., 2002); 0.43 ppb/h at a mountain site in



541 Hohenpeissenberg, Germany (Acker et al., 2006b); 0.5 ppb/h in a forest near Jülich,  
542 Germany (Kleffmann, 2005); 0.7 ppb/h in a outskirts of Paris, France; 0.77 ppb/h in a  
543 polluted rural area of the Pearl River Delta, China (Li et al., 2012); 0.98 ppb/h at an  
544 urban site in Xi'an, China (Huang et al., 2017); 1.0 ppb/h in a suburban area of  
545 Beijing, China (Yang et al., 2014); 1.7 ppb/h in an urban area of Santiago, Chile  
546 (Elshorbany et al., 2009); 2.95 ppb/h in the urban atmosphere of Jinan, China (Li et al.,  
547 2018); and 3.05 ppb/h at an urban site in Beijing, China (Wang et al., 2017).

548

549 The highest noontime  $P_{\text{unknown}}$  value is  $1.73 \text{ ppb h}^{-1}$  in spring, followed by  $1.15 \text{ ppb h}$   
550  $^{-1}$  in winter,  $1.0 \text{ ppb h}^{-1}$  in summer and  $0.77 \text{ ppb h}^{-1}$  in autumn, unlike the  
551 seasonal variation of  $\text{NO}_2$ ; and  $P_{\text{unknown}}$  shows an increase towards noon, this  
552 production rate is higher before noon than after noon, which is also distinguished  
553 from the diurnal pattern of  $\text{NO}_2$ . These results indicate that the production of daytime  
554 HONO is different from the heterogeneous formation from  $\text{NO}_2$  at night. Hence, we  
555 perform a correlation analysis between noontime  $P_{\text{unknown}}$  and related parameters to  
556 determine the potential unknown daytime source of HONO (Table 4).  $P_{\text{unknown}}$  is  
557 better correlated with  $\text{NO}_2 \cdot \text{UVB}$  than with  $\text{NO}_2$  or UVB alone in winter, spring and  
558 autumn ( $p=0.05$ ), perhaps associated with the photo-enhanced converting from  $\text{NO}_2$   
559 to HONO (George et al., 2005; Stemmler et al., 2006; Stemmler et al., 2007), and this  
560 is the reason for  $P_{\text{unknown}}$  normalized by  $\text{NO}_2$  following the steps of UVB, showing a  
561 peak around noontime in different seasons (Fig. 8). The average value of  $P_{\text{unknown}}$   
562 normalized by  $\text{NO}_2$  is  $0.1 \text{ h}^{-1}$ , over 18 times greater than the nighttime conversion rate  
563 ( $0.0055 \text{ h}^{-1}$ ), also implying that  $P_{\text{unknown}}$  cannot be explained by the  $\text{NO}_2$ -to-HONO  
564 mechanism at night. Assuming that the height of a well-mixed boundary layer around  
565 remain constant for each day,  $\text{UVB} \cdot \text{NO}_2$  and  $\text{UVB} \cdot \text{NO}_2 \cdot \text{PM}_{2.5}$  could be proxies for  
566 photo-induced heterogeneous reactions of  $\text{NO}_2$  on ground and aerosol surfaces,  
567 respectively. In winter and spring, the correlation numbers of  $P_{\text{unknown}}$  with  $\text{UVB} \cdot \text{NO}_2$   
568 are similar to those of  $P_{\text{unknown}}$  with  $\text{UVB} \cdot \text{NO}_2 \cdot \text{PM}_{2.5}$ , while if we only consider  
569  $\text{UVB} \cdot \text{NO}_2$  instead of  $\text{UVB} \cdot \text{NO}_2 \cdot \text{PM}_{2.5}$  in summer and autumn, the correlations



570 significantly increase ( $p=0.05$ ). We cannot be sure which surfaces (ground or aerosol)  
571 are more important to the hypothetical photo-heterogeneous reaction of  $\text{NO}_2$  based on  
572 the present study. The photolysis of particulate nitrates ( $\text{NO}_3^-$ ) as a source of HONO  
573 (Ye et al., 2016; Ye et al., 2017) cannot be determined if it is momentous in our study,  
574 since the correlation between  $P_{\text{unknown}}$  and  $\text{UVB} \cdot \text{NO}_2$  isn't superior to the correlation  
575 between  $P_{\text{unknown}}$  and  $\text{UVB}$  multiplied by  $\text{PM}_{2.5}$  or other aerosol compounds. The  
576 comparisons of correlation coefficients shown above follow the method provided by  
577 Meng et al. (1992). Overall, it seems that the sealed source of daytime HONO is  
578 optically controlled, although we are not sure what the actual mechanism is.

579

#### 580 *4. Estimation of the contribution from different sources*

581

582 From this and previous studies, we can concluded that not only the concentration of  
583 ambient HONO but also the sources of HONO have temporal and spatial patterns,  
584 which is supposed to be considered in model studies. Nocturnal HONO is selected to  
585 discuss the monthly variations of HONO sources in detail without the uncertainties of  
586 daytime HONO formation and the influences of HONO photolysis. The  
587 heterogeneous reaction of  $\text{NO}_2$  on aerosol produces a considerable portion of HONO  
588 in relatively polluted months (Dec.-May), but contributes very little less than nothing  
589 in clean months (Jun.-Oct.), as seen in section 3.3.3. Coincidentally, direct emissions  
590 from burning processes of HONO decrease from their peak values from winter to  
591 summer (section 3.2). However, the monthly averaged ratios of HONO and  $\text{NO}_x$  are  
592 highest in summer, which conflicts with two sources mentioned above.

593

594 As is known, higher  $\text{NO}_2$ -to-HONO conversion level or other  $\text{NO}_x$ -independent  
595 sources can cause an increase in the HONO/ $\text{NO}_x$  ratio. For the case of a mostly  
596 constant surface with low reactivity due to the long-term exposure to oxidizing gases  
597 and radiation, the yield of nighttime HONO from  $\text{NO}_2$  reacting on ground surfaces  
598 could be imprecisely assumed to be unchanged. Thus, soil nitrite formed through  
599 microbial activities, especially nitrification by ammonia-oxidizing bacteria  
600 ( $\text{NH}_4^+ \rightarrow \text{NO}_2^-$ ) (Su et al., 2011; Oswald et al., 2013), is adopted to be an source for



601 atmospheric HONO in this study, considering the nearby presence of some grassland  
602 and natural vegetation mosaics. Although we do not directly measure HONO  
603 emissions from soil, the observed ammonia can represent its monthly average  
604 intensity, based on the following hypothesis: the dominant source of  $\text{NH}_3$  is from soil,  
605 especially from fertilizers ( $\text{NH}_4^+ \rightarrow \text{NH}_3$ ) for a good correlation between ammonia and  
606 temperature in the site ( $r=0.63$ ,  $p=0.01$ ), omitting the contributions of livestock to  
607  $\text{NH}_3$  since there is only a small poultry facility within 10 km of this site (Meng et al.,  
608 2011;Huang et al., 2012;Behera et al., 2013). Combustion sources (vehicles, industry,  
609 biomass burning) should contribute only a fraction of  $\text{NH}_3$  seeing that  $\text{NH}_3$  is not  
610 related to  $\text{NO}_x$  or CO in our study. Moreover, the release of both HONO and  $\text{NH}_3$   
611 depend on the strength of microbial activities, fertilizing amount, and soil properties  
612 (e.g., temperature, acidity and water content of soil). Although the processes of  
613 HONO and  $\text{NH}_3$  emission from soil may not be completely synchronized, the  
614 seasonal patterns for each should be consistent.

615

616 Until now, we can separate the sources of HONO into four parts: (1) combustion  
617 emissions from vehicles and industries ( $\text{HONO}_{\text{emi}}$ ) with a constant emitted  
618 HONO/ $\text{NO}_x$  ratio of 0.79%; (2) conversion of  $\text{NO}_2$  to HONO on the ground surfaces  
619 ( $\text{HONO}_{\text{grd}}$ ) with a constant but unknown yield  $x_1$ ; (3) conversion of  $\text{NO}_2$  to HONO on  
620 aerosol surfaces ( $\text{HONO}_{\text{aer}}$ ) with a  $\text{PM}_{2.5}$ -dependent yield ( $\text{HONO}_{\text{aer}}/\text{NO}_2$ ); and (4)  
621 emission from soil ( $\text{HONO}_{\text{soi}}$ ), expressed by corrected  $\text{NH}_3$  multiplied by an unknown  
622 coefficient  $x_2$ . The corrected  $\text{NH}_3$  is obtained by subtracting combustion emission  
623 from total observed ammonia. Ammonia from combustion is found to be proportional  
624 to simultaneous CO (Meng et al., 2011;Chang et al., 2016), and a proportion of 0.3%,  
625 which is in the lower quantile of the  $\text{NH}_3/\text{CO}$  ratios in fresh air masses (for hourly  
626 data:  $\text{NO}/\text{NO}_x > 0.75$ ;  $\text{UVB}=0$ ;  $\text{temperature} < 5^\circ\text{C}$ ) is used from our measurements.  
627 Substituting monthly average values of measured HONO,  $\text{NO}_2$ ,  $\text{PM}_{2.5}$ ,  $\text{NH}_3$ , and CO  
628 into Eq. (9) by assuming that  $\text{HONO}_{\text{tot}}$  is equal to  $\text{HONO}_{\text{obs}}$ , we can get an  
629 overdetermined system of equations with 11 equations with 2 unknowns (excluding  
630 means of related parameters from February), finally achieving an approximate



631 solution ( $x_1=1.89%$ ,  $x_2=1.62%$ ) by the method of ordinary least squares.

632

633 Fig. 9 shows that an average of 36% of HONO is produced heterogeneously on  
634 ground surfaces without perceptible temporal variations, but the contribution of this  
635 source is overtaken by  $\text{NO}_2$  converting to HONO on aerosols in January  
636 (approximately 40% of HONO), and was exceeded by soil emission in July and  
637 August (approximately 40% of HONO). The seasonal variations of HONO from  
638 different pathways at night indicate that short-term observations may just capture a  
639 small part of the total picture when exploring the source mechanisms of HONO. The  
640 total HONO concentration ( $\text{HONO}_{\text{tot}}$ ) is the sum of derived HONO from the four  
641 sources listed above. The good correlation between  $\text{HONO}_{\text{tot}}$  and  $\text{HONO}_{\text{obs}}$  and the  
642 low mean normalized error of  $\text{HONO}_{\text{tot}}$  to  $\text{HONO}_{\text{obs}}$  indicate that our assumption  
643 regarding nocturnal HONO sources is reasonable. It should be noted that the slope of  
644 the linearly fitted line between  $\text{HONO}_{\text{corr}}/\text{NO}_2$  and  $\text{PM}_{2.5}$  in spring ( $r=0.74$ ,  
645 slope= $0.68\%$ ) is much higher than that in winter ( $r=0.60$ , slope= $0.20\%$ ), but we just  
646 use a mean slope of  $0.26\%$  to evaluate aerosol effects throughout the year, this may  
647 be why our method underestimates HONO in March and April and overestimates  
648 HONO in January, and revealing that the mass concentration of  $\text{PM}_{2.5}$  is not the only  
649 factor affecting formation of HONO on aerosols. Besides, lack consideration of the  
650 impact of RH and temperature on  $\text{NO}_2$ -to-HONO conversion and of seasonal  
651 variations in ground surface properties, uncertainties of  $\text{NO}_2$ -to-HONO conversion  
652 mechanisms and of combustion HONO emissions, and lack direct observation for soil  
653 emitted HONO, could all result in the bias between  $\text{HONO}_{\text{tot}}$  and  $\text{HONO}_{\text{obs}}$ , so more  
654 studies on the detailed mechanism of various HONO sources need to be performed.

655



$$\begin{aligned}
 \frac{[\text{HONO}_{\text{grd}}]}{[\text{NO}_2]} &= x_1 \\
 \frac{[\text{HONO}_{\text{aer}}]}{[\text{NO}_2]} &= 0.26\% \times [\text{PM}_{2.5}] \\
 \frac{[\text{HONO}_{\text{emi}}]}{[\text{NO}_x]} &= 0.79\% \\
 \frac{[\text{HONO}_{\text{soi}}]}{[\text{NH}_3] - 0.3\% \times [\text{CO}]} &= x_2 \\
 \text{HONO}_{\text{tot}} &= \text{HONO}_{\text{emi}} + \text{HONO}_{\text{soi}} + \text{HONO}_{\text{grd}} + \text{HONO}_{\text{aer}}
 \end{aligned}
 \tag{11}$$

657

658 **5. Conclusions**

659

660 Continuous field measurement of HONO over one year was conducted at SORPES  
 661 station in Nanjing in the western Yangtze River Delta (YRD), China, from December,  
 662 2017 to December, 2018. The observed seasonal average of HONO concentrations are  
 663 in the range of 0.45-1.04 ppb, which are comparable to those in other urban or  
 664 suburban regions and appears to be of vital importance to atmospheric oxidation as  
 665 the photolysis rate of HONO is over 2 times that of ozone at daytime. HONO and  
 666 NO<sub>x</sub> have coincident monthly variations peaking in December and decreasing to the  
 667 lowest value in August, and have similar diurnal pattern with the highest value in the  
 668 early morning and a low point before dusk, both indicating that NO<sub>x</sub> is a crucial  
 669 precursor of HONO.

670

671 Combustion emissions contribute an average of 23% to nocturnal HONO  
 672 concentrations, with an average emission ratio  $\Delta\text{HONO}/\Delta\text{NO}_x$  of 0.79%. During  
 673 the nighttime, the dominant source of RH-dependent HONO could be the  
 674 heterogeneous reaction of NO<sub>2</sub> on wet ground or aerosol surfaces with a mean  
 675 estimated conversion rate of 0.0055 h<sup>-1</sup>. During the daytime, a missing HONO source  
 676 with an average strength of 1.13 ppb h<sup>-1</sup> was identified around noon, contributing  
 677 more than 75% of the production of HONO and seeming to be photo-enhanced.  
 678 HONO released from soil is adopted to discuss the seasonal changes of nocturnal  
 679 HONO, and can contribute 40% to HONO during summer. Ground formation



680 provides a major part of HONO at roughly constant proportion of 36%. The uptake of  
681 NO<sub>2</sub> on aerosol surface could generate the greatest amount of HONO during heavily  
682 polluted periods (e.g. January). Our results draw a complete picture of the sources of  
683 HONO during different seasons, and demonstrated the needs of long-term and  
684 comprehensive observations to improve the understanding of HONO chemistry.

#### 685 **Author contribution**

686 W.N. and A.D. designed the study; Y.L. and W.N. wrote the manuscript; Y.L., Z.X.  
687 and R.X. collected the HONO data and contributed to the data analysis; T.W., Y.L.,  
688 L.W. and X.C. collected other related data, e.g. NH<sub>3</sub>, NO<sub>x</sub> and PM<sub>2.5</sub>.

#### 689 **Acknowledgments**

690 This work was mainly funded by the National Key R&D Program of China  
691 (2016YFC0202000 and 2016YFC0200500), and the National Natural Science  
692 Foundation of China (NSFC) project (D0512/41675145 and D0510/41605098). Data  
693 analysis was also supported by other NSFC projects (D0512/41875175 and  
694 D0510/41605098).

#### 695 **References**

- 696  
697 Acker, K., Möller, D., Auel, R., Wieprecht, W., and Kalaß, D.: Concentrations of nitrous acid,  
698 nitric acid, nitrite and nitrate in the gas and aerosol phase at a site in the emission zone during  
699 ESCOMPTE 2001 experiment, *Atmospheric Research*, 74, 507-524,  
700 10.1016/j.atmosres.2004.04.009, 2005.
- 701 Acker, K., Febo, A., Trick, S., Perrino, C., Bruno, P., Wiesen, P., Möller, D., Wieprecht, W.,  
702 Auel, R., and Giusto, M.: Nitrous acid in the urban area of Rome, *Atmos. Environ.*, 40,  
703 3123-3133, 2006a.
- 704 Acker, K., Möller, D., Wieprecht, W., Meixner, F. X., Bohn, B., Gilge, S., Plass-Dülmer, C.,  
705 and Berresheim, H.: Strong daytime production of OH from HNO<sub>2</sub> at a rural mountain site,  
706 *Geophysical Research Letters*, 33, 10.1029/2005gl024643, 2006b.
- 707 Ackermann, R.: Auswirkungen von Kraftfahrzeugemissionen in der urbanen Atmosphäre,  
708 Dissertation. de, 2000.
- 709 Alicke, B.: Impact of nitrous acid photolysis on the total hydroxyl radical budget during the  
710 Limitation of Oxidant Production/Pianura Padana Produzione di Ozono study in Milan,  
711 *Journal of Geophysical Research*, 107, 10.1029/2000jd000075, 2002.



- 712 Alicke, B., Platt, U., and Stutz, J.: Impact of nitrous acid photolysis on the total hydroxyl  
713 radical budget during the Limitation of Oxidant Production/Pianura Padana Produzione di  
714 Ozono study in Milan, *Journal of Geophysical Research: Atmospheres*, 107, LOP 9-1-LOP  
715 9-17, 2002.
- 716 Alicke, B.: OH formation by HONO photolysis during the BERLIOZ experiment, *Journal of*  
717 *Geophysical Research*, 108, 10.1029/2001jd000579, 2003.
- 718 Ammann, M., Kalberer, M., Jost, D., Tobler, L., Rossler, E., Pigué, D., Gaggeler, H., and  
719 Baltensperger, U.: Heterogeneous production of nitrous acid on soot in polluted airmasses,  
720 *NATURE*, 395, 157-160, 10.1038/25965, 1998.
- 721 Ammann, M., Rossler, E., Strekowski, R., and George, C.: Nitrogen dioxide multiphase  
722 chemistry: uptake kinetics on aqueous solutions containing phenolic compounds, *Phys Chem*  
723 *Chem Phys*, 7, 2513-2518, 10.1039/b501808k, 2005.
- 724 Atkinson, R.: Atmospheric chemistry of VOCs and NO<sub>x</sub>, *Atmos. Environ.*, 34, 2063-2101,  
725 2000.
- 726 Atkinson, R., Baulch, D., Cox, R., Crowley, J., Hampson, R., Hynes, R., Jenkin, M., Rossi,  
727 M., and Troe, J.: Evaluated kinetic and photochemical data for atmospheric chemistry:  
728 Volume I-gas phase reactions of O<sub>x</sub>, HO<sub>x</sub>, NO<sub>x</sub> and SO<sub>x</sub> species, *Atmospheric chemistry*  
729 *and physics*, 4, 1461-1738, 2004.
- 730 Aubin, D. G., and Abbatt, J. P.: Interaction of NO<sub>2</sub> with hydrocarbon soot: Focus on HONO  
731 yield, surface modification, and mechanism, *The Journal of Physical Chemistry A*, 111,  
732 6263-6273, 2007.
- 733 Becker, K. H., Kleffmann, J., Kurtenbach, R., and Wiesen, P.: Solubility of nitrous acid  
734 (HONO) in sulfuric acid solutions, *The Journal of Physical Chemistry*, 100, 14984-14990,  
735 1996.
- 736 Behera, S. N., Sharma, M., Aneja, V. P., and Balasubramanian, R.: Ammonia in the  
737 atmosphere: a review on emission sources, atmospheric chemistry and deposition on  
738 terrestrial bodies, *Environ Sci Pollut Res Int*, 20, 8092-8131, 10.1007/s11356-013-2051-9,  
739 2013.
- 740 Bernard, F., Cazaunau, M., Gosselin, B., Zhou, B., Zheng, J., Liang, P., Zhang, Y., Ye, X.,  
741 Daele, V., Mu, Y., Zhang, R., Chen, J., and Mellouki, A.: Measurements of nitrous acid  
742 (HONO) in urban area of Shanghai, China, *Environ Sci Pollut Res Int*, 23, 5818-5829,  
743 10.1007/s11356-015-5797-4, 2016.
- 744 Canfield, D. E., Glazer, A. N., and Falkowski, P. G.: The Evolution and Future of Earth's  
745 Nitrogen Cycle, *Science*, 330, 192-196, 10.1126/science.1186120, 2010.
- 746 Chang, Y., Zou, Z., Deng, C., Huang, K., Collett, J. L., Lin, J., and Zhuang, G.: The  
747 importance of vehicle emissions as a source of atmospheric ammonia in the megacity of  
748 Shanghai, *Atmospheric Chemistry and Physics*, 16, 3577, 2016.
- 749 Cheung, J., Li, Y., Boniface, J., Shi, Q., Davidovits, P., Worsnop, D., Jayne, J., and Kolb, C.:  
750 Heterogeneous interactions of NO<sub>2</sub> with aqueous surfaces, *The Journal of Physical Chemistry*  
751 *A*, 104, 2655-2662, 2000.
- 752 Coe, H., and Gallagher, M.: Measurements of dry deposition of NO<sub>2</sub> to a Dutch heathland  
753 using the eddy-correlation technique, *Quarterly Journal of the Royal Meteorological Society*,



- 754 118, 767-786, 1992.
- 755 Cui, L., Li, R., Zhang, Y., Meng, Y., Fu, H., and Chen, J.: An observational study of nitrous  
756 acid (HONO) in Shanghai, China: The aerosol impact on HONO formation during the haze  
757 episodes, *Sci Total Environ*, 630, 1057-1070, 10.1016/j.scitotenv.2018.02.063, 2018.
- 758 Dillon, M. B.: Chemical evolution of the Sacramento urban plume: Transport and oxidation,  
759 2002.
- 760 Ding, A., Nie, W., Huang, X., Chi, X., Sun, J., Kerminen, V.-M., Xu, Z., Guo, W., Petäjä, T.,  
761 Yang, X., Kulmala, M., and Fu, C.: Long-term observation of air pollution-weather/climate  
762 interactions at the SORPES station: a review and outlook, *Frontiers of Environmental Science  
763 & Engineering*, 10, 10.1007/s11783-016-0877-3, 2016.
- 764 Ding, A. J., Fu, C. B., Yang, X. Q., Sun, J. N., Zheng, L. F., Xie, Y. N., Herrmann, E., Nie,  
765 W., Petäjä, T., Kerminen, V. M., and Kulmala, M.: Ozone and fine particle in the western  
766 Yangtze River Delta: an overview of 1 yr data at the SORPES station, *Atmospheric  
767 Chemistry and Physics*, 13, 5813-5830, 10.5194/acp-13-5813-2013, 2013.
- 768 Dusanter, S., Vimal, D., Stevens, P., Volkamer, R., and Molina, L.: Measurements of OH and  
769 HO<sub>2</sub> concentrations during the MCMA-2006 field campaign–Part 1: Deployment of the  
770 Indiana University laser-induced fluorescence instrument, *Atmospheric Chemistry and  
771 Physics*, 9, 1665-1685, 2009.
- 772 Elshorbany, Y. F., Kurtenbach, R., Wiesen, P., Lissi, E., Rubio, M., Villena, G., Gramsch, E.,  
773 Rickard, A., Pilling, M., and Kleffmann, J.: Oxidation capacity of the city air of Santiago,  
774 Chile, *Atmospheric Chemistry and Physics*, 9, 2257-2273, 2009.
- 775 Finlayson-Pitts, B. J., and Pitts Jr, J. N.: *Chemistry of the upper and lower atmosphere: theory,  
776 experiments, and applications*, Elsevier, 1999.
- 777 Finlayson-Pitts, B. J., Wingen, L. M., Sumner, A. L., Syomin, D., and Ramazan, K. A.: The  
778 heterogeneous hydrolysis of NO<sub>2</sub> in laboratory systems and in outdoor and indoor  
779 atmospheres: An integrated mechanism, *Physical Chemistry Chemical Physics*, 5, 223-242,  
780 10.1039/b208564j, 2003.
- 781 George, C., Streckowski, R. S., Kleffmann, J., Stemmler, K., and Ammann, M.:  
782 Photoenhanced uptake of gaseous NO<sub>2</sub> on solid organic compounds: a photochemical source  
783 of HONO?, *Faraday Discussions*, 130, 195, 10.1039/b417888m, 2005.
- 784 Grassian, V.: Chemical reactions of nitrogen oxides on the surface of oxide, carbonate, soot,  
785 and mineral dust particles: Implications for the chemical balance of the troposphere, *The  
786 Journal of Physical Chemistry A*, 106, 860-877, 2002.
- 787 Han, C., Liu, Y., and He, H.: Heterogeneous reaction of NO<sub>2</sub> with soot at different relative  
788 humidity, *Environmental Science and Pollution Research*, 24, 21248-21255,  
789 10.1007/s11356-017-9766-y, 2017.
- 790 Hao, N., Zhou, B., Chen, D., and Chen, L.-m.: Observations of nitrous acid and its relative  
791 humidity dependence in Shanghai, *Journal of Environmental Sciences*, 18, 910-915,  
792 10.1016/s1001-0742(06)60013-2, 2006.
- 793 Harrison, R. M., Peak, J. D., and Collins, G. M.: Tropospheric cycle of nitrous acid, *Journal  
794 of Geophysical Research: Atmospheres*, 101, 14429-14439, 1996.
- 795 He, Y., Zhou, X., Hou, J., Gao, H., and Bertman, S. B.: Importance of dew in controlling the



- 796 air-surface exchange of HONO in rural forested environments, *Geophysical Research Letters*,  
797 33, 10.1029/2005gl024348, 2006.
- 798 Heland, J., Kleefmann, J., Kurtenbach, R., and Wiesen, P. A new instrument to  
799 measure gaseous nitrous acid (HONO) in the atmosphere, *Environmental Science &*  
800 *Technology*, 35, 3207-3212, 2001.
- 801 Hendrick, F., Müller, J. F., Clémer, K., Wang, P., De Mazière, M., Fayt, C., Gielen, C.,  
802 Hermans, C., Ma, J. Z., Pinardi, G., Stavrakou, T., Vlemmix, T., and Van Roozendaal, M.:  
803 Four years of ground-based MAX-DOAS observations of HONO and  
804 NO<sub>2</sub> in the Beijing area, *Atmospheric Chemistry and Physics*, 14,  
805 765-781, 10.5194/acp-14-765-2014, 2014.
- 806 Hirokawa, J., Kato, T., and Mafuné, F.: Uptake of gas-phase nitrous acid by pH-controlled  
807 aqueous solution studied by a wetted wall flow tube, *The Journal of Physical Chemistry A*,  
808 112, 12143-12150, 2008.
- 809 Hou, S., Tong, S., Ge, M., and An, J.: Comparison of atmospheric nitrous acid during severe  
810 haze and clean periods in Beijing, China, *Atmos. Environ.*, 124, 199-206,  
811 10.1016/j.atmosenv.2015.06.023, 2016.
- 812 Huang, R. J., Yang, L., Cao, J., Wang, Q., Tie, X., Ho, K. F., Shen, Z., Zhang, R., Li, G., Zhu,  
813 C., Zhang, N., Dai, W., Zhou, J., Liu, S., Chen, Y., Chen, J., and O'Dowd, C. D.:  
814 Concentration and sources of atmospheric nitrous acid (HONO) at an urban site in Western  
815 China, *Sci Total Environ.*, 593-594, 165-172, 10.1016/j.scitotenv.2017.02.166, 2017.
- 816 Huang, X., Song, Y., Li, M., Li, J., Huo, Q., Cai, X., Zhu, T., Hu, M., and Zhang, H.: A  
817 high-resolution ammonia emission inventory in China, *Global Biogeochemical Cycles*, 26,  
818 n/a-n/a, 10.1029/2011gb004161, 2012.
- 819 Jarvis, D. L., Leaderer, B. P., Chinn, S., and Burney, P. G.: Indoor nitrous acid and  
820 respiratory symptoms and lung function in adults, *Thorax*, 60, 474-479,  
821 10.1136/thx.2004.032177, 2005.
- 822 Jenkin, M. E., Cox, R. A., and Williams, D. J.: Laboratory studies of the kinetics of formation  
823 of nitrous acid from the thermal reaction of nitrogen dioxide and water vapour, *Atmos.*  
824 *Environ.*, 22, 487-498, 1988.
- 825 Kalberer, M., Ammann, M., Arens, F., Gäggeler, H. W., and Baltensperger, U.:  
826 Heterogeneous formation of nitrous acid (HONO) on soot aerosol particles, *Journal of*  
827 *Geophysical Research: Atmospheres*, 104, 13825-13832, 10.1029/1999jd900141, 1999.
- 828 Kanaya, Y., Cao, R., Akimoto, H., Fukuda, M., Komazaki, Y., Yokouchi, Y., Koike, M.,  
829 Tanimoto, H., Takegawa, N., and Kondo, Y.: Urban photochemistry in central Tokyo: 1.  
830 Observed and modeled OH and HO<sub>2</sub> radical concentrations during the winter and summer of  
831 2004, *Journal of Geophysical Research*, 112, 10.1029/2007jd008670, 2007.
- 832 Khalizov, A. F., Cruz-Quinones, M., and Zhang, R.: Heterogeneous reaction of NO<sub>2</sub> on fresh  
833 and coated soot surfaces, *The Journal of Physical Chemistry A*, 114, 7516-7524, 2010.
- 834 Kirchner, U., Scheer, V., and Vogt, R.: FTIR spectroscopic investigation of the mechanism  
835 and kinetics of the heterogeneous reactions of NO<sub>2</sub> and HNO<sub>3</sub> with soot, *The Journal of*  
836 *Physical Chemistry A*, 104, 8908-8915, 2000.
- 837 Kirchstetter, T., Harley, R., and Littlejohn, D.: Measurement of Nitrous Acid in Motor



- 838 Vehicle Exhaust, *Environmental Science & Technology Letters*, 30, 2843-2849,  
839 10.1021/es960135y, 1996.
- 840 Kleffmann, J., Becker, K., and Wiesen, P.: Heterogeneous NO<sub>2</sub> conversion processes on acid  
841 surfaces: Possible atmospheric implications, *Atmos. Environ.*, 32, 2721-2729,  
842 10.1016/S1352-2310(98)00065-X, 1998.
- 843 Kleffmann, J., Becker, K. H., Lackhoff, M., and Wiesen, P.: Heterogeneous conversion of  
844 NO<sub>2</sub> on carbonaceous surfaces, *Physical Chemistry Chemical Physics*, 1, 5443-5450, 1999.
- 845 Kleffmann, J.: Daytime formation of nitrous acid: A major source of OH radicals in a forest,  
846 *Geophysical Research Letters*, 32, 10.1029/2005gl022524, 2005.
- 847 Kleffmann, J., Lörzer, J. C., Wiesen, P., Kern, C., Trick, S., Volkamer, R., Rodenas, M., and  
848 Wirtz, K.: Intercomparison of the DOAS and LOPAP techniques for the detection of nitrous  
849 acid (HONO), *Atmos. Environ.*, 40, 3640-3652, 10.1016/j.atmosenv.2006.03.027, 2006.
- 850 Kurtenbach, R., Becker, K., Gomes, J., Kleffmann, J., Lorzer, J., Spittler, M., Wiesen, P.,  
851 Ackermann, R., Geyer, A., and Platt, U.: Investigations of emissions and heterogeneous  
852 formation of HONO in a road traffic tunnel, *Atmos. Environ.*, 35, 3385-3394,  
853 10.1016/S1352-2310(01)00138-8, 2001.
- 854 Lammel, G., and Cape, J. N.: Nitrous Acid and Nitrite in the Atmosphere, *CHEMICAL*  
855 *SOCIETY REVIEWS*, 25, 361-369, 10.1039/cs9962500361, 1996.
- 856 Lammel, G.: Formation of nitrous acid: parameterisation and comparison with observations,  
857 Max-Planck-Institut für Meteorologie, 1999.
- 858 Lee, J. D., Whalley, L. K., Heard, D. E., Stone, D., Dunmore, R. E., Hamilton, J. F., Young,  
859 D. E., Allan, J. D., Laufs, S., and Kleffmann, J.: Detailed budget analysis of HONO in central  
860 London reveals a missing daytime source, *Atmospheric Chemistry and Physics*, 16,  
861 2747-2764, 10.5194/acp-16-2747-2016, 2016.
- 862 Lee, Y., and Schwartz, S.: Reaction kinetics of nitrogen dioxide with liquid water at low  
863 partial pressure, *The Journal of Physical Chemistry*, 85, 840-848, 1981.
- 864 Li, D., Xue, L., Wen, L., Wang, X., Chen, T., Mellouki, A., Chen, J., and Wang, W.:  
865 Characteristics and sources of nitrous acid in an urban atmosphere of northern China: Results  
866 from 1-yr continuous observations, *Atmos. Environ.*, 182, 296-306,  
867 10.1016/j.atmosenv.2018.03.033, 2018.
- 868 Li, X., Brauers, T., Häseler, R., Bohn, B., Fuchs, H., Hofzumahaus, A., Holland, F., Lou, S.,  
869 Lu, K. D., Rohrer, F., Hu, M., Zeng, L. M., Zhang, Y. H., Garland, R. M., Su, H., Nowak, A.,  
870 Wiedensohler, A., Takegawa, N., Shao, M., and Wahner, A.: Exploring the atmospheric  
871 chemistry of nitrous acid (HONO) at a rural site in Southern China, *Atmospheric Chemistry*  
872 *and Physics*, 12, 1497-1513, 10.5194/acp-12-1497-2012, 2012.
- 873 Liu, Y., Han, C., Ma, J., Bao, X., and He, H.: Influence of relative humidity on heterogeneous  
874 kinetics of NO<sub>2</sub> on kaolin and hematite, *Phys Chem Chem Phys*, 17, 19424-19431,  
875 10.1039/c5cp02223a, 2015.
- 876 Lu, K. D., Rohrer, F., Holland, F., Fuchs, H., Bohn, B., Brauers, T., Chang, C. C., Häseler, R.,  
877 Hu, M., Kita, K., Kondo, Y., Li, X., Lou, S. R., Nehr, S., Shao, M., Zeng, L. M., Wahner, A.,  
878 Zhang, Y. H., and Hofzumahaus, A.: Observation and modelling of OH and HO<sub>2</sub>  
879 concentrations in the Pearl River Delta 2006: a missing OH source in a VOC rich atmosphere,



- 880 Atmospheric Chemistry and Physics, 12, 1541-1569, 10.5194/acp-12-1541-2012, 2012.
- 881 Lu, K. D., Hofzumahaus, A., Holland, F., Bohn, B., Brauers, T., Fuchs, H., Hu, M., Häsel, R., Kita, K., Kondo, Y., Li, X., Lou, S. R., Oebel, A., Shao, M., Zeng, L. M., Wahner, A.,  
882 Zhu, T., Zhang, Y. H., and Rohrer, F.: Missing OH source in a suburban environment near  
883 Beijing: observed and modelled OH and HO<sub>2</sub> concentrations in summer 2006,  
884 Atmospheric Chemistry and Physics, 13, 1057-1080, 10.5194/acp-13-1057-2013, 2013.
- 886 Meng, X.-L., Rosenthal, R., and Rubin, D. B.: Comparing correlated correlation coefficients,  
887 Psychological bulletin, 111, 172, 1992.
- 888 Meng, Z., Lin, W., Jiang, X., Yan, P., Wang, Y., Zhang, Y., Jia, X., and Yu, X.:  
889 Characteristics of atmospheric ammonia over Beijing, China, Atmospheric Chemistry and  
890 Physics, 11, 6139-6151, 2011.
- 891 Meusel, H., Kuhn, U., Reiffs, A., Mallik, C., Harder, H., Martinez, M., Schuladen, J., Bohn,  
892 B., Parchatka, U., Crowley, J. N., Fischer, H., Tomsche, L., Novelli, A., Hoffmann, T.,  
893 Janssen, R. H. H., Hartogensis, O., Pikridas, M., Vrekoussis, M., Bourtsoukidis, E., Weber, B.,  
894 Lelieveld, J., Williams, J., Pöschl, U., Cheng, Y., and Su, H.: Daytime formation of nitrous  
895 acid at a coastal remote site in Cyprus indicating a common ground source of atmospheric  
896 HONO and NO, Atmospheric Chemistry and Physics, 16, 14475-14493,  
897 10.5194/acp-16-14475-2016, 2016.
- 898 Michoud, V., Colomb, A., Borbon, A., Miet, K., Beekmann, M., Camredon, M., Aumont, B.,  
899 Perrier, S., Zapf, P., Siour, G., Ait-Helal, W., Afif, C., Kukui, A., Furger, M., Dupont, J. C.,  
900 Haefelin, M., and Doussin, J. F.: Study of the unknown HONO daytime source at a European  
901 suburban site during the MEGAPOLI summer and winter field campaigns, Atmospheric  
902 Chemistry and Physics, 14, 2805-2822, 10.5194/acp-14-2805-2014, 2014.
- 903 Nie, W., Ding, A. J., Xie, Y. N., Xu, Z., Mao, H., Kerminen, V. M., Zheng, L. F., Qi, X. M.,  
904 Huang, X., Yang, X. Q., Sun, J. N., Herrmann, E., Petäjä, T., Kulmala, M., and Fu, C. B.:  
905 Influence of biomass burning plumes on HONO chemistry in eastern China, Atmospheric  
906 Chemistry and Physics, 15, 1147-1159, 10.5194/acp-15-1147-2015, 2015.
- 907 Oswald, R., Behrendt, T., Ermel, M., Wu, D., Su, H., Cheng, Y., Breuninger, C., Moravek, A.,  
908 Mougín, E., and Delon, C.: HONO emissions from soil bacteria as a major source of  
909 atmospheric reactive nitrogen, Science, 341, 1233-1235, 2013.
- 910 Pagsberg, P., Bjergbakke, E., Ratajczak, E., and Sillesen, A.: Kinetics of the gas phase  
911 reaction OH + NO (+ M) → HONO (+ M) and the determination of the UV absorption cross  
912 sections of HONO, Chemical physics letters, 272, 383-390, 1997.
- 913 Park, J. Y., and Lee, Y. N.: Solubility and decomposition kinetics of nitrous acid in aqueous  
914 solution, The Journal of Physical Chemistry, 92, 6294-6302, 1988.
- 915 Perner, D., and Platt, U.: Detection of nitrous acid in the atmosphere by differential optical  
916 absorption, Geophysical Research Letters, 6, 917-920, doi:10.1029/GL006i012p00917, 1979.
- 917 Platt, U., Perner, D., Harris, G. W., Winer, A. M., and Pitts, J. N.: Observations of nitrous  
918 acid in an urban atmosphere by differential optical absorption, Nature, 285, 312-314,  
919 10.1038/285312a0, 1980.
- 920 Qi, X. M., Ding, A. J., Nie, W., Petäjä, T., Kerminen, V. M., Herrmann, E., Xie, Y. N., Zheng,  
921 L. F., Manninen, H., Aalto, P., Sun, J. N., Xu, Z. N., Chi, X. G., Huang, X., Boy, M.,



- 922 Virkkula, A., Yang, X. Q., Fu, C. B., and Kulmala, M.: Aerosol size distribution and new  
923 particle formation in the western Yangtze River Delta of China: 2 years of measurements at  
924 the SORPES station, *Atmospheric Chemistry and Physics*, 15, 12445-12464,  
925 10.5194/acp-15-12445-2015, 2015.
- 926 Qin, M., Xie, P., Su, H., Gu, J., Peng, F., Li, S., Zeng, L., Liu, J., Liu, W., and Zhang, Y.: An  
927 observational study of the HONO-NO<sub>2</sub> coupling at an urban site in Guangzhou City, South  
928 China, *Atmos. Environ.*, 43, 5731-5742, 10.1016/j.atmosenv.2009.08.017, 2009.
- 929 Rappenglück, B., Lubertino, G., Alvarez, S., Golovko, J., Czader, B., and Ackermann, L.:  
930 Radical precursors and related species from traffic as observed and modeled at an urban  
931 highway junction, *Journal of the Air & Waste Management Association*, 63, 1270-1286,  
932 10.1080/10962247.2013.822438, 2013.
- 933 Reisinger, A. R.: Observations of HNO<sub>2</sub> in the polluted winter atmosphere: possible  
934 heterogeneous production on aerosols, *Atmos. Environ.*, 34, 3865-3874, 2000.
- 935 Richter, A., Burrows, J. P., Nuss, H., Granier, C., and Niemeier, U.: Increase in tropospheric  
936 nitrogen dioxide over China observed from space, *Nature*, 437, 129-132,  
937 10.1038/nature04092, 2005.
- 938 Rohde, R. A., and Muller, R. A.: Air Pollution in China: Mapping of Concentrations and  
939 Sources, *PLoS One*, 10, e0135749, 10.1371/journal.pone.0135749, 2015.
- 940 Rohrer, F., and Berresheim, H.: Strong correlation between levels of tropospheric hydroxyl  
941 radicals and solar ultraviolet radiation, *Nature*, 442, 184-187, 10.1038/nature04924, 2006.
- 942 Saliba, N., Yang, H., and Finlayson-Pitts, B.: Reaction of gaseous nitric oxide with nitric acid  
943 on silica surfaces in the presence of water at room temperature, *The Journal of Physical  
944 Chemistry A*, 105, 10339-10346, 2001.
- 945 Seinfeld, J. H., and Pandis, S. N.: *Atmospheric chemistry and physics: from air pollution to  
946 climate change*, John Wiley & Sons, 2016.
- 947 Shao, P., Xin, J., An, J., Kong, L., Wang, B., Wang, J., Wang, Y., and Wu, D.: The empirical  
948 relationship between PM<sub>2.5</sub> and AOD in Nanjing of the Yangtze River Delta, *Atmospheric  
949 Pollution Research*, 8, 233-243, 10.1016/j.apr.2016.09.001, 2017.
- 950 Shen, Y., Virkkula, A., Ding, A., Wang, J., Chi, X., Nie, W., Qi, X., Huang, X., Liu, Q.,  
951 Zheng, L., Xu, Z., Petäjä, T., Aalto, P. P., Fu, C., and Kulmala, M.: Aerosol optical properties  
952 at SORPES in Nanjing, east China, *Atmospheric Chemistry and Physics*, 18, 5265-5292,  
953 10.5194/acp-18-5265-2018, 2018.
- 954 Sleiman, M., Gundel, L. A., Pankow, J. F., Jacob, P., 3rd, Singer, B. C., and Destailats, H.:  
955 Formation of carcinogens indoors by surface-mediated reactions of nicotine with nitrous acid,  
956 leading to potential thirdhand smoke hazards, *Proc Natl Acad Sci U S A*, 107, 6576-6581,  
957 10.1073/pnas.0912820107, 2010.
- 958 Sörgel, M., Regelin, E., Bozem, H., Diesch, J. M., Drewnick, F., Fischer, H., Harder, H., Held,  
959 A., Hosaynali-Beygi, Z., Martinez, M., and Zetzsch, C.: Quantification of the unknown  
960 HONO daytime source and its relation to NO<sub>2</sub>, *Atmospheric Chemistry and Physics*, 11,  
961 10433-10447, 10.5194/acp-11-10433-2011, 2011.
- 962 Stemmler, K., Ammann, M., Donders, C., Kleffmann, J., and George, C.: Photosensitized  
963 reduction of nitrogen dioxide on humic acid as a source of nitrous acid, *Nature*, 440, 195-198,



- 964 10.1038/nature04603, 2006.
- 965 Stemmler, K., Ndour, M., Elshorbany, Y., Kleffmann, J., D'anna, B., George, C., Bohn, B.,  
966 and Ammann, M.: Light induced conversion of nitrogen dioxide into nitrous acid on  
967 submicron humic acid aerosol, *Atmospheric Chemistry and Physics*, 7, 4237-4248, 2007.
- 968 Stutz, J., Kim, E. S., Platt, U., Bruno, P., Perrino, C., and Febo, A.: UV-visible absorption  
969 cross sections of nitrous acid, *Journal of Geophysical Research: Atmospheres*, 105,  
970 14585-14592, 10.1029/2000jd900003, 2000.
- 971 Stutz, J., Alicke, B., and Neftel, A.: Nitrous acid formation in the urban atmosphere: Gradient  
972 measurements of NO<sub>2</sub> and HONO over grass in Milan, Italy, *Journal of Geophysical Research*,  
973 107, 10.1029/2001jd000390, 2002.
- 974 Stutz, J., Alicke, B., Ackermann, R., Geyer, A., Wang, S., White, A. B., Williams, E. J.,  
975 Spicer, C. W., and Fast, J. D.: Relative humidity dependence of HONO chemistry in urban  
976 areas, *Journal of Geophysical Research: Atmospheres*, 109, n/a-n/a, 10.1029/2003jd004135,  
977 2004.
- 978 Su, H., Cheng, Y. F., Cheng, P., Zhang, Y. H., Dong, S., Zeng, L. M., Wang, X., Slanina, J.,  
979 Shao, M., and Wiedensohler, A.: Observation of nighttime nitrous acid (HONO) formation at  
980 a non-urban site during PRIDE-PRD2004 in China, *Atmos. Environ.*, 42, 6219-6232,  
981 10.1016/j.atmosenv.2008.04.006, 2008a.
- 982 Su, H., Cheng, Y. F., Shao, M., Gao, D. F., Yu, Z. Y., Zeng, L. M., Slanina, J., Zhang, Y. H.,  
983 and Wiedensohler, A.: Nitrous acid (HONO) and its daytime sources at a rural site during the  
984 2004 PRIDE-PRD experiment in China, *Journal of Geophysical Research*, 113,  
985 10.1029/2007jd009060, 2008b.
- 986 Su, H., Cheng, Y., Oswald, R., Behrendt, T., Trebs, I., Meixner, F. X., Andreae, M. O., Cheng,  
987 P., Zhang, Y., and Pöschl, U.: Soil nitrite as a source of atmospheric HONO and OH radicals,  
988 *Science*, 333, 1616-1618, 2011.
- 989 Sumner, A. L., Menke, E. J., Dubowski, Y., Newberg, J. T., Penner, R. M., Hemminger, J. C.,  
990 Wingen, L. M., Brauers, T., and Finlayson-Pitts, B. J.: The nature of water on surfaces of  
991 laboratory systems and implications for heterogeneous chemistry in the troposphere, *Physical  
992 Chemistry Chemical Physics*, 6, 10.1039/b308125g, 2004.
- 993 Sun, P., Nie, W., Chi, X., Xie, Y., Huang, X., Xu, Z., Qi, X., Xu, Z., Wang, L., Wang, T.,  
994 Zhang, Q., and Ding, A.: Two years of online measurement of fine particulate nitrate in the  
995 western Yangtze River Delta: influences of thermodynamics and  
996 N<sub>2</sub>O<sub>5</sub> hydrolysis, *Atmospheric Chemistry  
997 and Physics*, 18, 17177-17190, 10.5194/acp-18-17177-2018, 2018.
- 998 Tong, S., Hou, S., Zhang, Y., Chu, B., Liu, Y., He, H., Zhao, P., and Ge, M.: Comparisons of  
999 measured nitrous acid (HONO) concentrations in a pollution period at urban and suburban  
1000 Beijing, in autumn of 2014, *Science China Chemistry*, 58, 1393-1402,  
1001 10.1007/s11426-015-5454-2, 2015.
- 1002 Underwood, G., Song, C., Phadnis, M., Carmichael, G., and Grassian, V.: Heterogeneous  
1003 reactions of NO<sub>2</sub> and HNO<sub>3</sub> on oxides and mineral dust: A combined laboratory and  
1004 modeling study, *Journal of Geophysical Research: Atmospheres*, 106, 18055-18066, 2001.
- 1005 VandenBoer, T., Markovic, M., Sanders, J., Ren, X., Pusede, S., Browne, E., Cohen, R.,



- 1006 Zhang, L., Thomas, J., and Brune, W.: Evidence for a nitrous acid (HONO) reservoir at the  
1007 ground surface in Bakersfield, CA, during CalNex 2010, *Journal of Geophysical Research:*  
1008 *Atmospheres*, 119, 9093-9106, 2014a.
- 1009 VandenBoer, T. C., Young, C. J., Talukdar, R. K., Markovic, M. Z., Brown, S. S., Roberts, J.  
1010 M., and Murphy, J. G.: Nocturnal loss and daytime source of nitrous acid through reactive  
1011 uptake and displacement, *Nature Geoscience*, 8, 55-60, 10.1038/ngeo2298, 2014b.
- 1012 Villena, G., Kleffmann, J., Kurtenbach, R., Wiesen, P., Lissi, E., Rubio, M. A., Croxatto, G.,  
1013 and Rappenglück, B.: Vertical gradients of HONO, NO<sub>x</sub> and O<sub>3</sub> in Santiago de Chile, *Atmos.*  
1014 *Environ.*, 45, 3867-3873, 10.1016/j.atmosenv.2011.01.073, 2011a.
- 1015 Villena, G., Wiesen, P., Cantrell, C. A., Flocke, F., Fried, A., Hall, S. R., Hornbrook, R. S.,  
1016 Knapp, D., Kosciuch, E., Mauldin, R. L., McGrath, J. A., Montzka, D., Richter, D., Ullmann,  
1017 K., Walega, J., Weibring, P., Weinheimer, A., Staebler, R. M., Liao, J., Huey, L. G., and  
1018 Kleffmann, J.: Nitrous acid (HONO) during polar spring in Barrow, Alaska: A net source of  
1019 OH radicals?, *Journal of Geophysical Research*, 116, 10.1029/2011jd016643, 2011b.
- 1020 Wang, J., Zhang, X., Guo, J., Wang, Z., and Zhang, M.: Observation of nitrous acid (HONO)  
1021 in Beijing, China: Seasonal variation, nocturnal formation and daytime budget, *Sci Total*  
1022 *Environ.*, 587-588, 350-359, 10.1016/j.scitotenv.2017.02.159, 2017.
- 1023 Wang, S.: Atmospheric observations of enhanced NO<sub>2</sub>-HONO conversion on mineral dust  
1024 particles, *Geophysical Research Letters*, 30, 10.1029/2003gl017014, 2003.
- 1025 Wang, S., Zhou, R., Zhao, H., Wang, Z., Chen, L., and Zhou, B.: Long-term observation of  
1026 atmospheric nitrous acid (HONO) and its implication to local NO<sub>2</sub> levels in Shanghai, China,  
1027 *Atmos. Environ.*, 77, 718-724, 10.1016/j.atmosenv.2013.05.071, 2013.
- 1028 Wentzell, J. J. B., Schiller, C. L., and Harris, G. W.: Measurements of HONO during  
1029 BAQS-Met, *Atmospheric Chemistry and Physics*, 10, 12285-12293,  
1030 10.5194/acp-10-12285-2010, 2010.
- 1031 Wong, K. W., Oh, H. J., Lefer, B. L., Rappenglück, B., and Stutz, J.: Vertical profiles of  
1032 nitrous acid in the nocturnal urban atmosphere of Houston, TX, *Atmospheric Chemistry and*  
1033 *Physics*, 11, 3595-3609, 10.5194/acp-11-3595-2011, 2011.
- 1034 Xie, Y., Ding, A., Nie, W., Mao, H., Qi, X., Huang, X., Xu, Z., Kerminen, V.-M., Petäjä, T.,  
1035 Chi, X., Virkkula, A., Boy, M., Xue, L., Guo, J., Sun, J., Yang, X., Kulmala, M., and Fu, C.:  
1036 Enhanced sulfate formation by nitrogen dioxide: Implications from in situ observations at the  
1037 SORPES station, *Journal of Geophysical Research: Atmospheres*, 120, 12679-12694,  
1038 10.1002/2015jd023607, 2015.
- 1039 Xu, Z., Wang, T., Xue, L. K., Louie, P. K. K., Luk, C. W. Y., Gao, J., Wang, S. L., Chai, F.  
1040 H., and Wang, W. X.: Evaluating the uncertainties of thermal catalytic conversion in  
1041 measuring atmospheric nitrogen dioxide at four differently polluted sites in China, *Atmos.*  
1042 *Environ.*, 76, 221-226, 10.1016/j.atmosenv.2012.09.043, 2013.
- 1043 Xu, Z., Wang, T., Wu, J., Xue, L., Chan, J., Zha, Q., Zhou, S., Louie, P. K. K., and Luk, C. W.  
1044 Y.: Nitrous acid (HONO) in a polluted subtropical atmosphere: Seasonal variability, direct  
1045 vehicle emissions and heterogeneous production at ground surface, *Atmos. Environ.*, 106,  
1046 100-109, 10.1016/j.atmosenv.2015.01.061, 2015.
- 1047 Xu, Z., Huang, X., Nie, W., Chi, X., Xu, Z., Zheng, L., Sun, P., and Ding, A.: Influence of



- 1048 synoptic condition and holiday effects on VOCs and ozone production in the Yangtze River  
1049 Delta region, China, *Atmos. Environ.*, 168, 112-124, 10.1016/j.atmosenv.2017.08.035, 2017.
- 1050 Xu, Z., Huang, X., Nie, W., Shen, Y., Zheng, L., Xie, Y., Wang, T., Ding, K., Liu, L., Zhou,  
1051 D., Qi, X., and Ding, A.: Impact of Biomass Burning and Vertical Mixing of Residual-Layer  
1052 Aged Plumes on Ozone in the Yangtze River Delta, China: A Tethered-Balloon Measurement  
1053 and Modeling Study of a Multiday Ozone Episode, *Journal of Geophysical Research:*  
1054 *Atmospheres*, 123, 11,786-711,803, 10.1029/2018jd028994, 2018.
- 1055 Yang, Q., Su, H., Li, X., Cheng, Y., Lu, K., Cheng, P., Gu, J., Guo, S., Hu, M., Zeng, L., Zhu,  
1056 T., and Zhang, Y.: Daytime HONO formation in the suburban area of the megacity Beijing,  
1057 China, *Science China Chemistry*, 57, 1032-1042, 10.1007/s11426-013-5044-0, 2014.
- 1058 Ye, C., Zhou, X., Pu, D., Stutz, J., Festa, J., Spolaor, M., Tsai, C., Cantrell, C., Mauldin, R. L.,  
1059 3rd, Campos, T., Weinheimer, A., Hornbrook, R. S., Apel, E. C., Guenther, A., Kaser, L.,  
1060 Yuan, B., Karl, T., Haggerty, J., Hall, S., Ullmann, K., Smith, J. N., Ortega, J., and Knote, C.:  
1061 Rapid cycling of reactive nitrogen in the marine boundary layer, *Nature*, 532, 489-491,  
1062 10.1038/nature17195, 2016.
- 1063 Ye, C., Zhang, N., Gao, H., and Zhou, X.: Photolysis of Particulate Nitrate as a Source of  
1064 HONO and NO<sub>x</sub>, *Environ Sci Technol*, 51, 6849-6856, 10.1021/acs.est.7b00387, 2017.
- 1065 Yu, Y., Galle, B., Panday, A., Hodson, E., Prinn, R., and Wang, S.: Observations of high rates  
1066 of NO<sub>2</sub>-HONO conversion in the nocturnal atmospheric boundary layer in Kathmandu, Nepal,  
1067 *ATMOSPHERIC CHEMISTRY AND PHYSICS*, 9, 6401-6415, 10.5194/acp-9-6401-2009,  
1068 2009.
- 1069 Zhou, L., Wang, W., Hou, S., Tong, S., and Ge, M.: Heterogeneous uptake of nitrogen  
1070 dioxide on Chinese mineral dust, *J Environ Sci (China)*, 38, 110-118,  
1071 10.1016/j.jes.2015.05.017, 2015.
- 1072 Zhou, X., Civerolo, K., Dai, H., Huang, G., Schwab, J., and Demerjian, K.: Summertime  
1073 nitrous acid chemistry in the atmospheric boundary layer at a rural site in New York State,  
1074 *Journal of Geophysical Research: Atmospheres*, 107, ACH 13-11-ACH 13-11,  
1075 10.1029/2001jd001539, 2002.
- 1076 Zhou, X., Gao, H., He, Y., Huang, G., Bertman, S. B., Civerolo, K., and Schwab, J.: Nitric  
1077 acid photolysis on surfaces in low-NO<sub>x</sub> environments: Significant atmospheric implications,  
1078 *Geophysical Research Letters*, 30, n/a-n/a, 10.1029/2003gl018620, 2003.
- 1079 Zhou, X., Huang, G., Civerolo, K., Roychowdhury, U., and Demerjian, K. L.: Summertime  
1080 observations of HONO, HCHO, and O<sub>3</sub> at the summit of Whiteface Mountain, New York,  
1081 *Journal of Geophysical Research*, 112, 10.1029/2006jd007256, 2007.
- 1082 Zhou, X., Zhang, N., TerAvest, M., Tang, D., Hou, J., Bertman, S., Alaghmand, M., Shepson,  
1083 P. B., Carroll, M. A., Griffith, S., Dusanter, S., and Stevens, P. S.: Nitric acid photolysis on  
1084 forest canopy surface as a source for tropospheric nitrous acid, *Nature Geoscience*, 4, 440-443,  
1085 10.1038/ngeo1164, 2011.

**Tables****Table 1.** Sources and sinks for nitrous acid (HONO) in the troposphere.

Budget	Occurrence	Pathways	Abbr.
Sinks	Only daytime	$\text{HONO} + h\nu \xrightarrow{320-400\text{nm}} \text{OH} + \text{NO}$	R1
	Mainly daytime	$\text{HONO} + \text{OH} \rightarrow \text{NO}_2 + \text{H}_2\text{O}$	R2
	All day	Deposition/heterogeneous loss on aerosol	/
Sources	Mainly daytime	$\text{NO} + \text{OH} \xrightarrow{\text{M}} \text{HONO}$	R3
	Mainly nighttime	$2\text{NO}_{2(\text{g})} + \text{H}_2\text{O}_{(\text{ads})} \xrightarrow{\text{surf}} \text{HONO}_{(\text{g})} + \text{HNO}_{3(\text{ads})}$	R4
	Mainly daytime	$\text{NO}_{2(\text{g})} + \text{HC}_{\text{red}} \xrightarrow{\text{surf}} \text{HONO}_{(\text{g})} + \text{HC}_{\text{ox}}$	R5
	Only daytime	$\text{HNO}_3 / \text{NO}_3^- + h\nu \xrightarrow{\text{surf}} \text{HONO} / \text{NO}_2^- + \text{O}$	R6
	All day	Release of soil nitrite	/
	All day	Combustion emission (fossil and biomass)	/



**Table 2.** Overview of the measured HONO and NO<sub>x</sub> levels in Nanjing and comparison with other urban or suburban sites.

Location	Date	HONO(ppb)		NO <sub>2</sub> (ppb)		NO <sub>x</sub> (ppb)		HONO/NO <sub>2</sub>		HONO/NO <sub>x</sub>		Ref
		Night	Day	Night	Day	Night	Day	Night	Day	Night	Day	
Rome(Italy)	May-Jun 2001	1.00	0.15	27.2	4.0	51.2	4.2	0.037	0.038	0.020	0.036	1
Kathmandu(Nepal)	Jan-Feb 2003	1.74	0.35	17.9	8.6	20.1	13.0	0.097	0.041	0.087	0.027	2
Tokto(Japan)	Jan-Feb 2004	0.80	0.05	31.8	18.2	37.4	26.3	0.025	0.003	0.021	0.002	3
Santiago(Chile)	Mar 2005	3.00	1.50	30.0	20.0	200.0	40.0	0.100	0.075	0.015	0.038	4
Mexico City(Mexico)	Mar 2006	/	0.43	/	28.4	/	44.8	/	0.015	/	0.010	5
Houston(USA)	Sep 2006	0.50	0.10	20.0	10.0	/	/	0.025	0.010	/	/	6
Shanghai(China)	Oct 2009	1.50	1.00	41.9	30.0	/	/	0.038	0.032	/	/	7
Hongkong(China)	Aug 2011	0.66	0.70	21.8	18.1	29.3	29.3	0.031	0.042	0.025	0.028	8
	Nov 2011	0.95	0.89	27.2	29.0	37.2	40.6	0.034	0.030	0.028	0.021	
	Feb 2012	0.88	0.92	22.2	25.8	37.8	48.3	0.036	0.035	0.025	0.020	
	May 2012	0.33	0.40	14.7	15.0	19.1	21.1	0.022	0.030	0.019	0.022	
Beijing(China)	Oct–Nov 2014	1.75	0.93	37.6	35.3	94.5	53.4	0.047	0.026	0.019	0.017	9
Xi'an(China)	Jul–Aug 2015	0.51	1.57	15.4	24.7	/	/	0.033	0.062	/	/	10
Jinan(China)	Sep–Nov 2015	0.87	0.66	25.4	23.2	38.0	37.5	0.049	0.034	0.034	0.022	11
	Dec 2015–Feb 2016	2.15	1.35	41.1	34.6	78.5	64.8	0.056	0.047	0.034	0.031	
	Mar–May 2016	1.24	1.04	35.8	25.8	47.3	36.0	0.046	0.052	0.035	0.041	
	Jun–Aug 2016	1.20	1.01	22.5	19.0	29.1	25.8	0.106	0.079	0.060	0.049	
Nanjing(China)	Nov 2017–Nov 2018	0.80	0.57	18.9	13.9	24.9	19.3	0.045	0.044	0.041	0.036	this
	Dec–Feb(winter)	1.15	0.92	28.4	23.1	45.5	37.7	0.040	0.038	0.029	0.025	study
	Mar–May(spring)	0.76	0.59	17.4	12.9	19.1	15.9	0.048	0.049	0.046	0.042	
	Jun–Aug(summer)	0.56	0.34	12.5	7.7	13.5	9.1	0.048	0.051	0.046	0.045	
	Sep–Nov(autumn)	0.81	0.51	18.9	13.4	25.1	17.7	0.044	0.035	0.039	0.029	

1: Acker et al. (2006a); 2: Yu et al. (2009); 3: Kanaya et al. (2007); 4: Elshorbany et al. (2009); 5: Dusanter et al. (2009); 6: Wong et al. (2011); 7: Bernard et al. (2016); 8: Xu et al. (2015); 9: Tong et al. (2015); 10: Huang et al. (2017); 11: Li et al. (2018)



**Table 3.** the emission ratios  $\Delta\text{HONO}/\Delta\text{NO}_x$  in 55 selected fresh plumes emitted,  $r$  is the correlation coefficient between  $\Delta\text{HONO}$  and  $\Delta\text{NO}_x$ .

Start Time	Duration(min)	$\Delta\text{NO}/\Delta\text{NO}_x$	$r$	$\Delta\text{HONO}/\Delta\text{NO}_x(\%)$
11/15/2017 19:50	20	0.88	1.00	0.51
11/15/2017 20:50	30	1.00	0.97	0.42
11/15/2017 21:40	30	1.05	0.91	0.59
11/20/2017 21:50	110	0.91	0.90	0.79
11/21/2017 03:10	70	1.06	0.97	0.33
11/22/2017 05:40	30	1.14	0.93	0.35
11/23/2017 06:00	20	1.10	1.00	0.26
11/23/2017 19:30	110	1.09	0.92	0.67
11/24/2017 01:50	20	1.23	0.94	0.63
11/24/2017 17:20	20	0.91	0.98	0.48
11/28/2017 23:30	40	1.07	0.91	0.82
12/01/2017 01:10	120	1.07	0.91	0.64
12/03/2017 04:40	20	1.00	0.97	0.29
12/03/2017 23:00	30	1.12	0.93	1.91
12/07/2017 01:40	50	1.12	0.96	0.68
12/07/2017 05:40	20	0.85	0.93	0.42
12/07/2017 06:40	20	0.93	0.98	0.63
12/08/2017 19:40	20	1.08	0.99	0.98
12/08/2017 23:30	120	1.10	0.93	0.74
12/09/2017 20:20	120	0.89	0.90	0.74
12/11/2017 04:10	30	1.13	0.92	0.93
12/11/2017 07:10	20	1.13	0.94	0.97
12/17/2017 19:40	120	1.04	0.96	1.02
12/18/2017 03:10	90	1.09	0.94	0.59
12/20/2017 23:50	40	1.15	0.95	0.97
12/21/2017 01:20	40	1.21	0.90	0.98
12/21/2017 03:20	40	1.28	0.95	1.52
12/23/2017 07:10	30	0.96	0.97	1.09
12/23/2017 17:10	60	1.08	0.97	1.11
12/25/2017 02:00	110	1.05	0.91	0.81
12/26/2017 20:20	20	1.05	0.99	0.96
12/28/2017 22:40	100	1.02	0.92	1.29
01/10/2018 22:20	120	1.02	0.95	1.05
01/20/2018 23:50	120	1.20	0.93	1.36
01/21/2018 03:00	70	1.01	0.98	0.66



01/21/2018 19:20	50	1.03	0.98	0.38
01/30/2018 23:00	40	1.09	0.94	0.67
01/31/2018 04:10	70	1.16	0.90	0.67
01/31/2018 18:30	20	0.96	0.96	0.74
03/22/2018 03:30	110	0.87	0.94	0.44
04/10/2018 21:40	110	0.91	0.94	1.02
04/15/2018 20:50	50	0.94	0.97	1.47
04/27/2018 03:10	20	1.03	0.99	0.46
05/12/2018 19:20	30	0.88	0.92	1.21
05/30/2018 02:50	30	0.88	1.00	1.50
07/04/2018 02:20	20	0.91	1.00	0.42
09/28/2018 19:30	20	0.94	0.96	1.37
09/28/2018 21:40	40	0.99	0.98	0.80
09/29/2018 23:40	20	0.92	1.00	0.33
10/11/2018 01:20	120	0.96	0.92	0.65
10/22/2018 21:50	20	0.94	0.99	0.42
10/26/2018 22:50	110	1.07	0.90	0.92
10/27/2018 21:00	30	1.00	0.91	0.63
10/28/2018 00:00	70	0.99	0.91	0.58
11/21/2018 04:10	70	0.95	0.94	0.51

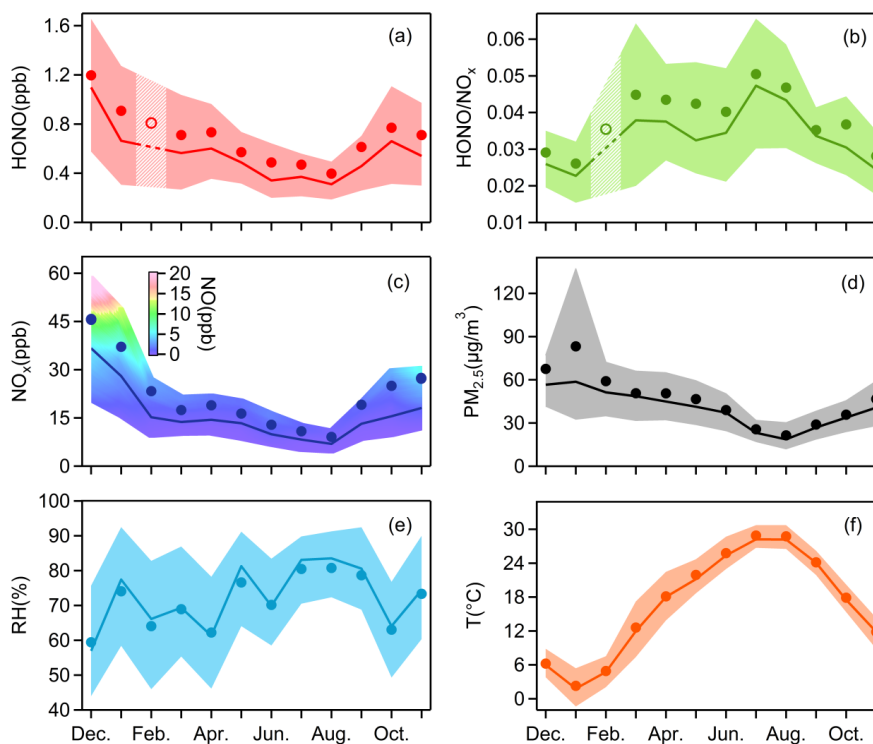
---

**Table 4.** Correlations of  $P_{\text{unknown}}$  against various parameters.

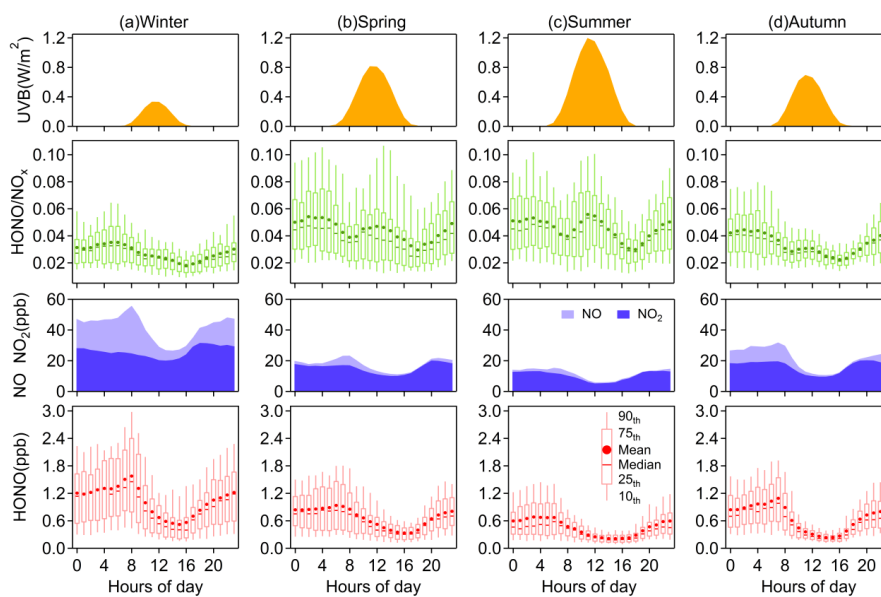
Parameters	Winter		Spring		Summer		Autumn	
	r	N	r	N	r	N	r	N
NO <sub>2</sub>	0.45	254	0.35	310	-0.04	423	0.23	381
PM <sub>2.5</sub>	0.41	254	0.45	310	0.18	423	0.31	381
NO <sub>3</sub> <sup>-</sup>	0.42	245	0.45	298	-0.03	409	0.21	373
SO <sub>4</sub> <sup>2-</sup>	0.33	236	0.29	298	0.12	413	0.21	368
NH <sub>4</sub> <sup>+</sup>	0.39	245	0.41	301	0.05	416	0.23	359
RH	0.02	254	-0.34	310	-0.42	423	-0.16	381
UVB	0.27	254	0.43	310	0.51	423	0.42	381
NO <sub>2</sub> *PM <sub>2.5</sub>	0.43	254	0.46	310	0.06	423	0.25	381
NO <sub>2</sub> *NO <sub>3</sub> <sup>-</sup>	0.43	245	0.45	298	-0.04	409	0.19	373
NO <sub>2</sub> *SO <sub>4</sub> <sup>2-</sup>	0.41	236	0.40	298	0.05	413	0.21	368
NO <sub>2</sub> *NH <sub>4</sub> <sup>+</sup>	0.42	245	0.45	301	0.01	416	0.20	359
UVB*NO <sub>2</sub>	0.65	254	0.67	310	0.48	423	0.59	381
UVB*PM <sub>2.5</sub>	0.58	254	0.64	310	0.50	423	0.64	381
UVB*NO <sub>3</sub> <sup>-</sup>	0.55	245	0.59	298	0.24	409	0.45	373
UVB*SO <sub>4</sub> <sup>2-</sup>	0.43	236	0.51	298	0.42	413	0.34	368
UVB*NH <sub>4</sub> <sup>+</sup>	0.51	245	0.57	301	0.32	416	0.49	359
NO <sub>2</sub> *UVB*PM <sub>2.5</sub>	0.59	254	0.65	310	0.37	423	0.49	381



1086 **Figures**  
1087



1088  
1089 **Fig. 1.** Monthly variations of (a) HONO, (b) HONO/NO<sub>x</sub>, (c) NO<sub>x</sub>, (d) PM<sub>2.5</sub>, (e) RH and (f) T.  
1090 The solid bold lines are median values, the markers indicate mean values, and the shaded areas  
1091 represent percentiles of 75% and 25%. In (a) and (b), values in February are linearly interpolated  
1092 based on the data from the months before and after, since there were only few days when HONO  
1093 was observed in February. In (c), the shaded area is colored by the 25<sup>th</sup> to the 75<sup>th</sup> percentiles of  
1094 NO.  
1095



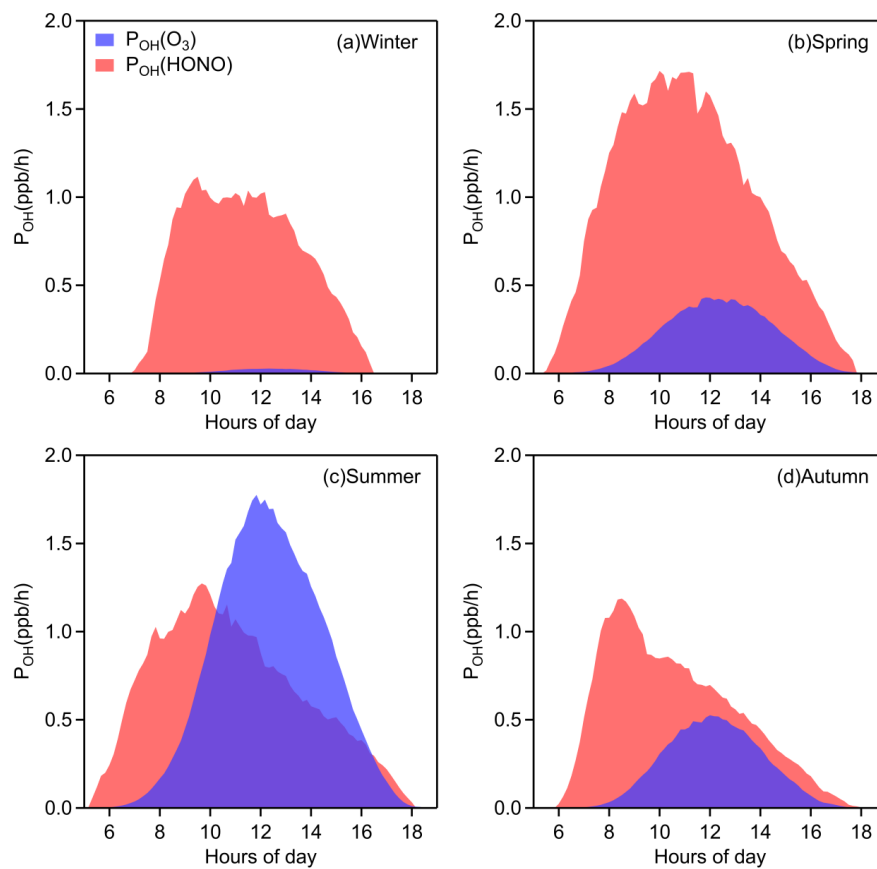
1096

1097

1098

1099

**Fig. 2.** Diurnal variations of HONO, NO, NO<sub>2</sub>, HONO/NO<sub>x</sub>, UVB in (a) winter, (b) spring, (c) summer, (d) autumn. NO, NO<sub>2</sub> and UVB values are displayed as their mean concentrations.



1100

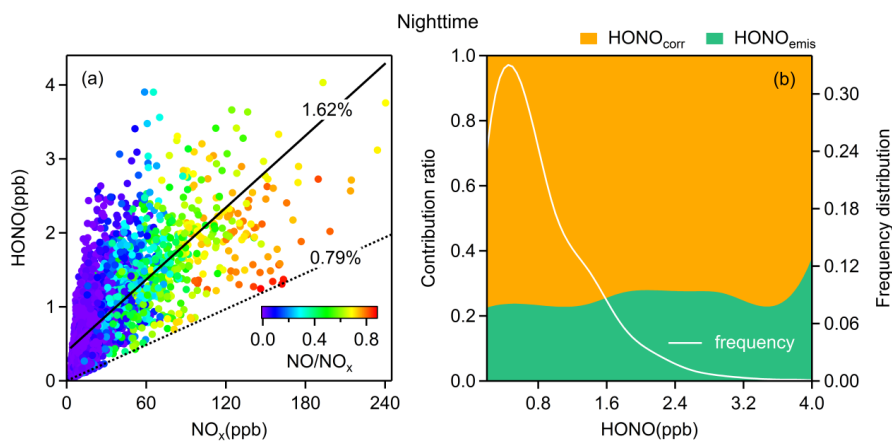
1101 **Fig. 3.** Average OH production rates from photolysis of HONO and O<sub>3</sub> in (a)winter, (b)spring,  
1102 (c)summer, and (d)autumn.

1103

1104

1105

1106



1107

1108 **Fig. 4.** (a) The relationship between HONO and NO<sub>x</sub> colored by NO/NO<sub>x</sub>. The dotted line is the  
 1109 emission ratio derived in this study and the solid line is obtained from simple linear fitting; (b)  
 1110 average emission contribution ratios for different concentrations of HONO and the frequency  
 1111 distribution of HONO concentrations. Both (a) and (b) are nighttime values.

1112

1113

1114

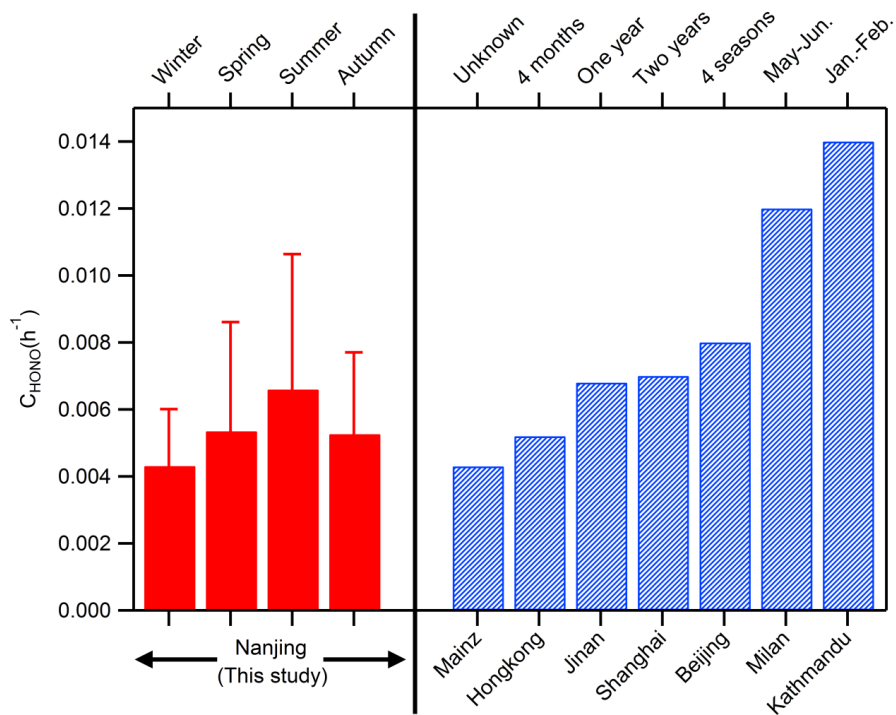
1115

1116

1117

1118

1119



1120

**Fig. 5.** Comparison of observed NO<sub>2</sub> to HONO conversion rates in cities: Nanjing (this study); Mainz (Lammel, 1999); Hongkong (Xu et al., 2015); Jinan (Li et al., 2018); Shanghai (Wang et al., 2013); Beijing (Wang et al., 2017); Milan (Alicke et al., 2002); and Kathmandu (Yu et al., 2009).

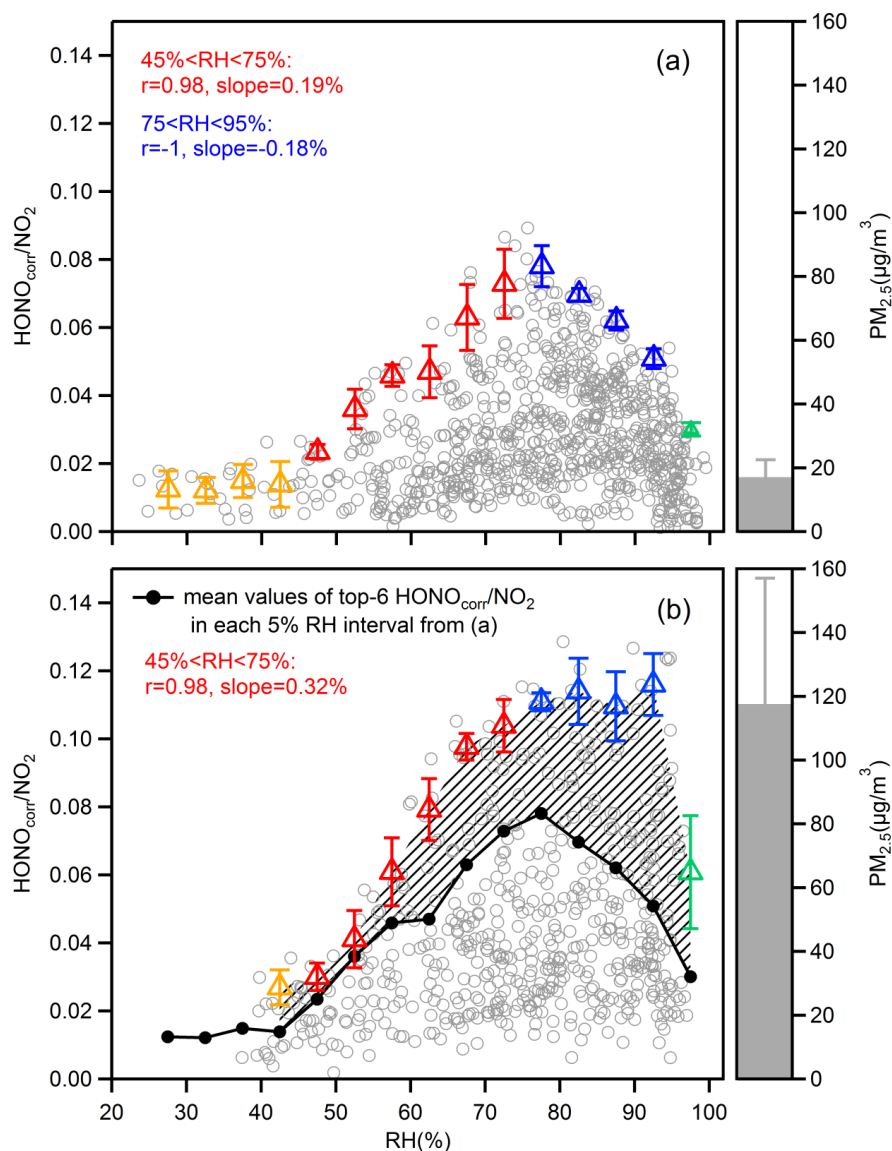


**Fig. 6.** Scatter plot of  $\text{HONO}_{\text{corr}}/\text{NO}_2$  and RH during nighttime, separating the data into (a) clean hours (hourly mean  $\text{PM}_{2.5} < 25 \mu\text{g}/\text{m}^3$ ) and (b) pollution hours (hourly mean  $\text{PM}_{2.5} > 75 \mu\text{g}/\text{m}^3$ ). Triangles are the averaged top-6  $\text{HONO}_{\text{corr}}/\text{NO}_2$  in each 5% RH interval, and the error bars are the standard deviations. The overall average concentrations of  $\text{PM}_{2.5}$  in (a) and (b) are shown to the right of the figure.

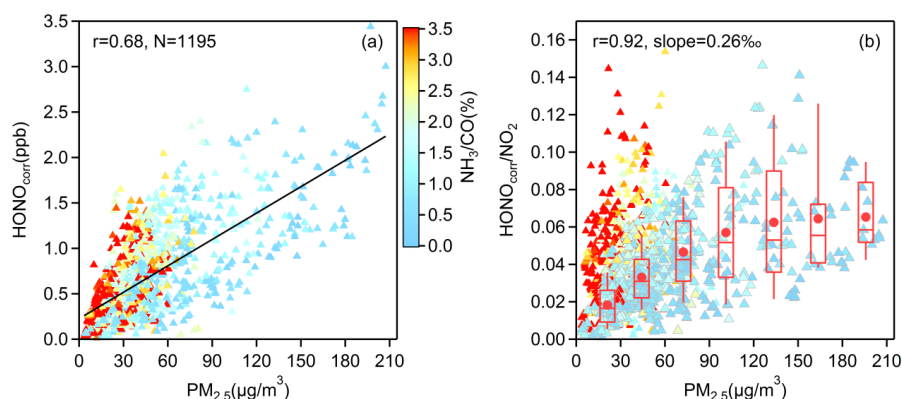


**Fig. 7.** The correlation between  $\text{HONO}_{\text{corr}}$  and  $\text{PM}_{2.5}$  (a), and the correlation between  $\text{HONO}_{\text{corr}}/\text{NO}_2$  and  $\text{PM}_{2.5}$  (b), all scatters come from the time (3:00–6:00 LT) when  $\text{HONO}_{\text{corr}}/\text{NO}_2$  reaches the pseudo steady state each night and are colored by  $\text{NH}_3/\text{CO}$ . In (b), the larger triangles with gray borders, depict the measured data from November to May, and the boxplot in each  $30 \mu\text{g}/\text{m}^3$  interval of  $\text{PM}_{2.5}$  is illustrated according to the same data, the red box boundaries represent interquartile range, the whiskers represent the 10%–90% percentile range, the horizontal red lines represent median values and the red markers represent mean values. The correlation coefficient and the slope of the linearly fitted line in (b) are derived from the average  $\text{HONO}_{\text{corr}}/\text{NO}_2$  and average  $\text{PM}_{2.5}$  in each box.

1121

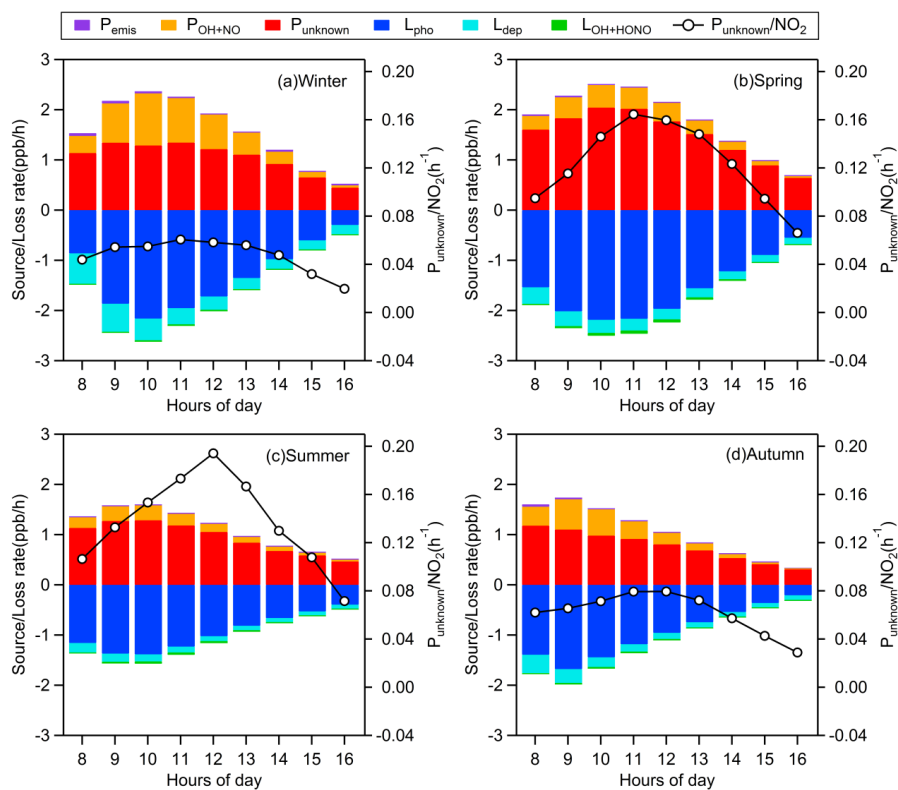


**Fig. 8.** Average daytime HONO budget and the missing source strength ( $P_{\text{unknown}}$ ) normalized by  $\text{NO}_2$  in (a) winter, (b) spring, (c) summer, and (d) autumn

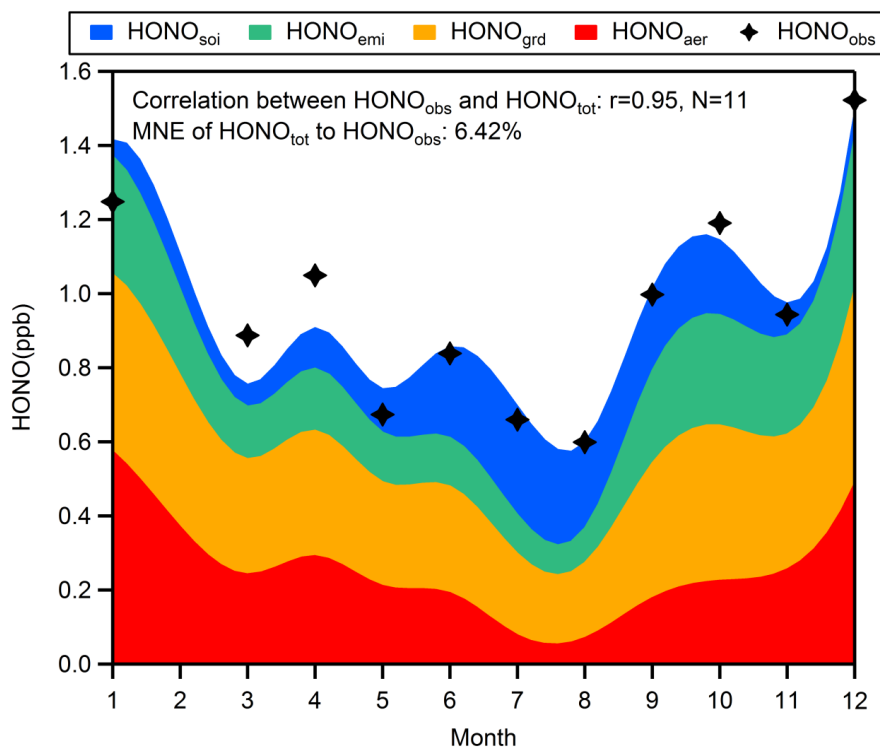


**Fig. 9.** Seasonal variations of 4 sources of mean HONO at night (3:00-6:00 LT). The mean normalized error (MNE) of  $\text{HONO}_{\text{tot}}$  to  $\text{HONO}_{\text{obs}}$  is 6.42%.